Journal of Alzheimer's Disease

MANUSCRIPT 09-304R1

"Extracellular AÎ² and cytotoxic glial activation induce significant entorhinal neuron loss in young PS1M146L/APP751SL mice"

DECISION LETTER

Your manuscript (09-304R1) has now been accepted in the Journal of Alzheimer's Disease. In keeping with the policy of JAD, you are cordially invited to become an Associate Editor of the journal. More information about the role of an Associate Editor is available at our website (http://www.j-alz.com/about/AErole.html); our structure is quite unique and centered on the open dissemination of novel ideas. If you choose to accept, your one-year term would begin January 1, 2010 and is renewable by future submissions or handling of manuscripts.

We look forward to a positive response.

We require financial disclosure statements from all authors for each accepted manuscript. Please log on to our new online disclosure system(http://www.j-alz.com/disclosures/) and enter your manuscript number(09-304R1). Select your name from the pull down list and complete the form. Please have all of your co-authors complete the form as well.

Additionally, please complete the Author Publication Fee Payment form(http://www.j-alz.com/about/publicationfee_Form.pdf). Please note that accepted manuscripts will not be moved into the production process until payment has been received. More information is available at our website: http://www.j-alz.com/about/publicationfee.html

Finally, please send your final formatted manuscript as a Word document and your figures as TIFs or JPGs to our Managing Editor, Beth
Kumar (editorial@j-alz.com).

Sincerely,
Mark A. Smith
Editor-in-Chief, JAD

Extracellular Aβ and cytotoxic glial activation induce significant entorhinal neuron loss in young PS1^{M146L}/APP^{751SL} mice

Ines Moreno-Gonzalez[1,4], David Baglietto-Vargas[1,4], Raquel Sanchez-Varo[1,4], Sebastián Jiménez[2,4,5], Laura Trujillo-Estrada[1,4], Elisabeth Sanchez-Mejias[1,4], Juan Carlos del Rio[2], Manuel Torres[2,4,5], Manuel Romero-Acebal[3,4], Diego Ruano[2,4,5], Marisa Vizuete[2,4,5], Javier Vitorica[2,4,5*] and Antonia Gutierrez[1,4*]

1- Dept. Biología Celular, Genética y Fisiología. Facultad de Ciencias, Universidad de Málaga, Spain
2- Dept. Bioquímica, Bromatologia, Toxicología y Medicina Legal, Facultad de Farmacia. Universidad de Sevilla, Spain
3- Servicio de Neurología, Hospital Universitario Virgen de la Victoria, Málaga
4- Centro de Investigación Biomédica en Red sobre Enfermedades Neurodegenerativas (CIBERNED), Spain.
5- Instituto de Biomedicina de Sevilla (IBiS)-Hospital Universitario Virgen del Rocío/CSIC/Universidad de Sevilla, Spain

*Co-Senior Authors

Running title: Early entorhinal neuron loss in PS1xAPP model

Corresponding Author:
Antonia Gutierrez, PhD
Dpto. Biología Celular, Genética y Fisiología
Facultad de Ciencias, Universidad de Málaga
Campus de Teatinos, 29071, Málaga, SPAIN
Phone: 34-952133344
Fax: 34-952131937
Email: agutierrez@uma.es

ABSTRACT

Here we demonstrated that extracellular, not intracellular, Aβ and the associated cytotoxic glial neuroinflammatory response are major contributors of early neuronal loss in a PS1xAPP model. A significant loss of principal (27%) and SOM/NPY (56-46%) neurons was found in the entorhinal cortex at 6 months of age. Loss of principal cells occurred selectively in deep layers (primarily layer V) whereas SOM/NPY cell loss was evenly distributed along the cortical column. Neither layer V pyramidal neurons nor SOM/NPY interneurons displayed intracellular Aβ immunoreactivity, even after formic acid retrieval, thus, extracellular factors should be preferentially implicated in this selective neurodegeneration. Amyloid deposits were mainly concentrated in deep layers at 4-6 months, and of relevance was the existence of a potentially cytotoxic inflammatory response (TNFalpha, TRAIL and iNOS mRNAs were upregulated). Moreover, non-plaques associated activated microglial cells and reactive astrocytes expressed TNFalpha and iNOS, respectively. At this age, in the hippocampus of same animals the extracellular Aβ induced a non-cytotoxic glial activation. The opposite glial activation, at the same chronological age, in entorhinal cortex and hippocampus strongly support different mechanisms of disease progression in these two regions highly affected by Aβ pathology.

Keywords: Alzheimer, transgenic, entorhinal cortex, neurodegeneration, neuroinflammation, amyloid, microglia

INTRODUCTION

Accumulation of extracellular beta-amyloid (Aβ) deposits, intracellular neurofibrillary tangles (NFTs) and progressive neurodegeneration, the major neuropathological lesions in Alzheimer's disease (AD) brains, occur with a regional and temporal defined pattern in vulnerable brain regions [1]. The entorhinal cortex is early affected by NFTs and Aβ deposits, and then these lesions spread to hippocampus and neocortical areas. Moreover, the earliest neuronal loss is detected in the entorhinal cortex [2]. As a key component of cortico-hippocampal networks, the entorhinal cortex plays an important role in memory processes. Superficial neurons (layers II and III) transfer processed cortical sensory information to the hippocampus via the perforant pathway and then deep entorhinal layers receive back information from CA1 and subiculum. Finally, these deep principal neurons (primarily from layer V) give rise to the major cortical and subcortical projections (for review see [3]. In addition, there are substantial intrinsic connections between deep and superficial layers [3-5]. Then, early entorhinal pathology impair this continuous information transfer and contribute to the cognitive decline in early phases of AD [6;7].

In AD, certain subpopulations of neurons are particularly affected, and specifically in the entorhinal cortex a selective layer vulnerability has been reported [2;8;9]. To study AD-related pathology and the mechanisms underlying neurodegeneration, mice expressing mutated human genes associated with the familial forms of AD are widely use. However, no pyramidal cell loss has been identified in these animal models at the initial stages of the pathology. We have previously reported the early and selective vulnerability of SOM/NPY

interneurons in the hippocampus of a PS1xAPP model [10]. These mice developed Aβ plaques since early ages [11;12]. However, hippocampal principal cell loss was detected at 17-18 months of age [10;12;13]. The scarce or delayed neuronal loss in most AD models, despite of extracellular/intracellular Aβ accumulation, is not well understood. To address this question we have recently reported the dual role (neuroprotective/neurotoxic) of microglial activation during the time course of the Aβ associated neuroinflammatory response in the hippocampus of PS1xAPP mice [14]. In this sense, at early ages the activated microglial cells displayed an alternative phenotype that could explain the limited neuronal loss (see also [15]). However, at advanced ages activated microglia exhibited a classical cytotoxic phenotype that could, probably, be responsible of the principal cell death.

Here, we have analyzed the entorhinal cortex at early ages in this PS1xAPP model. As in human patients, this region is affected earlier than hippocampus with significant loss of principal cells (in deep layers) and SOM and/or NPY interneurons (all layers). This early neurodegeneration coincided with extracellular, rather than intracellular, accumulation of Aβ and cytotoxic inflammatory response.

MATERIALS AND METHODS

Transgenic mice

The generation and initial characterization of the PS1 and PS1×APP transgenic (tg) mice has been reported previously [11]. PS1 tg mice (C57BL/6 background) over-expressed the mutated PS1M146L form under the control of the HMGCoA reductase promoter. PS1×APP double tg mice (C57BL/6 background) were obtained by crossing homozygotic PS1 tg mice with heterozygotic Thy1-APP751SL (Swedish -K670N, M671L- and London -V717I- FAD mutations) mice (Charles River, France). Mice represented F6–F10 offspring of heterozygous tg mice. Non-transgenic mice of the same genetic background and ages were used as controls. All animal experiments were carried out in accordance with the European Union regulations and approved by the committee of animal use for research at Malaga University.

Anatomical boundaries

The entorhinal cortex was anatomically defined according to previous studies [16];[17]. The entorhinal cortex is medially bordered by the parasubiculum and laterally by the perirhinal cortex; rostromedially it is bordered by the piriform cortex, whereas, caudodorsally, it is bordered by the postrhinal cortex. The entorhinal cortex is divided into two main areas, the lateral entorhinal area (LEnt) and the medial entorhinal area (MEnt). In the present study only the LEnt was analyzed and no subdivisions were made. The boundaries of the lateral entorhinal cortex in the mouse brain sections were identified on the basis of

their anatomical and cytoarchitectonic features, and using a standard mouse stereotaxic brain atlas [18].

Laser capture microdissection

Anesthetized 4- and 6-month old WT and PS1xAPP male mice (n=4/type/age) were killed by decapitation and brains were quickly removed and frozen. Brains were cut at 15 µm on a cryostat. Sections were collected onto Superfrost Plus slides (Fisher Scientific, Pittsburgh, PA) and stored at -80°C until use. The identification of lateral entorhinal cortex from brain sections lightly stained with hematoxilin was made according to the atlas of the mouse brain in stereotaxic coordinates [18]. Laser capture microdissection was performed using a Pix-Cell II instrument from Arcturus Engineering (Mountain View, CA). Cells were captured with the 30 µm laser setting and CapSure LCM Caps (Arcturus). The laser was set to a pulse of 60mW for 50ms. Entorhinal cortex and hippocampal stratus oriens were selectively captured from each section. After microdissection, the capture disk was cleared of nonspecifically adhering tissue using a CapSure Cleanup Pad (Arcturus).

RNA extraction and isolation

RNA was extracted using the PicoPure^{TM} RNA isolation kit. Capture disks with isolated material were microcentrifuged and incubated in the extraction buffer during 30 min at 42 ºC. Then, cell extract was centrifuged and frozen at -80 ºC. To isolate RNA, cell extracts were treated as indicated by the manufacturer (Arcturus). The integrity and the amount of purified RNA were analyzed using RNA 6000 Pico Assay kit (Agilent Technologies).

Retrotranscription and real-time PCR

The retrotranscription (RT) was done using High-Capacity cDNA Archive Kit (Applied Biosystems) following the manufacturer's recommendations. The RT-PCR was performed basically as described [10];[14] with the following modifications. Due to the low amount of tissue sample, the gene to be quantified (single gene per assay) was pre-amplified before quantitative RT-PCR (see [19]. Briefly, 1 or 5 µL of cDNA (in function of the expression levels of the gene to be quantified) were pre-amplified using 5 or 10 cycles of PCR (94 ºC for 4 min and 5-10 cycles of 94 ºC, 40 s, 60 ºC for 40 s and 72 ºC for 40 s followed by a final elongation period of 5 min at 72 ºC) using commercial Taqman^{TM} primers and Master Mix supplied from Applied Biosystems. After pre-amplification, the expression levels were assessed using the same set of Taqman TM probes in real-time RT-PCR experiments with an ABI Prism 7000 sequence detector (Applied Biosystems). The specificity of this protocol was always assessed by analyzing the PCR products on a 1.5 % agarose gel. Only experiments with a single and correct size PCR product were considered for quantification. On the other hand, the quantitative properties of this approach were also assessed by constructing concentration curves for each gene analyzed. The cDNA levels of the different mice were determined using beta-actin as housekeeper. The amplification of the housekeeper was done in parallel with the gene to be analyzed. The results were normalized using the beta-actin expression and the data were expressed respect to age-matched non-transgenic controls (see [14]).

Tissue preparation

After deep anesthesia with sodium pentobarbital (60 mg/kg), 2-, 4- and 6-month-old control (WT), PS1 and PS1×APP tg mice were perfused transcardially with 0.1M phosphate buffered saline (PBS), pH 7.4 followed by 4% paraformaldehyde, 75mM lysine, 10mM sodium metaperiodate in 0.1M phosphate buffer (PB), pH 7.4. Brains were post-fixed overnight in the same fixative at 4ºC, cryoprotected in 30% sucrose and sectioned (40µm thickness) in the coronal plane on a freezing microtome. Each experiment was composed of 4-6 sets of animals (each one containing one control, one PS1 tg mice and one PS1xAPP tg mice).

Immunohistochemistry

Serial sections from control (WT) and both tg mice (PS1 and PS1xAPP) were processed in parallel for light microscopy immunostaining (see [10;14]). Free-floating sections were first treated to inhibit endogenous peroxidases and block endogenous avidin, biotin and biotin-binding proteins. For immunolabeling sections were incubated with one of the following primary antibodies: anti-somatostatin (SOM) goat polyclonal (1:1000 dilution; Santa Cruz Biotechnology); anti-Neuropeptide Y (NPY) rabbit polyclonal (1:5000 dilution; Sigma); anti-Parvalbumin (PV) rabbit polyclonal (1/5000 dilution, Swant); anti-Calretinin (CR) rabbit polyclonal (1:5000 dilution; Swant); anti-VIP rabbit polyclonal (1:5000 dilution, Acris); anti-NeuN monoclonal antibody (1:1000 dilution; Chemicon); anti-hAPP rabbit polyclonal (1/20000; Sigma); anti-CD11b rat monoclonal (1/150000, Serotec), anti-Iba1 rabbit polyclonal (1:1000 dilution; Wako Chemical GmbH); anti-GFAP chicken polyclonal (1/2000 dilution,

Chemicon), anti-YM1 (AMCase) goat polyclonal (1:100 dilution, SantaCruz), anti-iNOS rabbit polyclonal (1:1000 dilution, Transduction Laboratories), anti-TNFalpha rat monoclonal (1:100 dilution; Abcam); anti-Aβ mouse monoclonal 6E10 (1:1500 dilution; Sigma); anti-Aβ1-40 rabbit polyclonal (1:40 dilution; Biosource), anti-Aβ1-42 rabbit polyclonal (1:40 dilution; Biosource), over 24 or 48 hours at room temperature. To retrieve intracellular Aβ, sections were pre-treated for 7 minutes with 85% formic acid before incubation with the anti-Aβ antibodies. For general antigen retrieval method sections were previously heated at 80°C for 20 minutes in 50mM citrate buffer pH 6.0. The tissue-bound primary antibody was then detected by incubating with the corresponding biotinylated secondary antibody (1:500 dilution, Vector Laboratories), and then with streptavidin-conjugated horseradish peroxidase (1:2000 dilution, Sigma–Aldrich). The peroxidase reaction was visualized with 0.05% 3-3-diaminobenzidine tetrahydrochloride (DAB), 0.03% nickel ammonium sulphate and 0.01% hydrogen peroxide in PBS. After DAB, sections immunolabeled for TNFalpha or Iba1 were incubated 3 minutes in a solution of 20% of Congo red. Specificity of the immune reactions was controlled by omitting the primary antisera.

For double SOM/NPY, GFAP-iNOS and hAPP/6E10 immunofluorescence labelings, sections were first sequentially incubated with the indicated primaries antibodies followed by the corresponding Alexa488/568 secondary antibodies (1:1000 dilution; Invitrogen). For double 6E10-Tomato lectin, sections after 6E10 immunofluorescence labeling were incubated for 1 hour at 37ºC with a solution of 5µg/ml biotinylated Tomato lectin (Sigma) followed by streptavidin-conjugated Alexa 568 (1:1000; Invitrogen). Sections

were examined under a confocal laser microscope (Leica TCS-NT) or Olympus BX-61 epifluorescent microscope.

For 5x multiple immunoperoxidase labeling, sections were first and sequentially incubated with anti-SOM, anti-PV, anti-CR and anti-VIP (all of them interneuronal markers) as described above. After the DAB-nickel reaction (dark blue end product), sections were then incubated 3 days with anti-NeuN monoclonal antibody (1:1000 dilution; Chemicon). The second immunoperoxidase reaction was developed with DAB only (brown reaction end product). The appropriate controls were performed to avoid any false positive immunostaining due to cross-reactivity between detection systems. To clearly discriminate the different streptavidin-peroxidase reactions, first one (for interneurons) was always developed with DAB-nickel (dark blue) solution whereas second one (NeuN) only with DAB (light brown). Moreover, the different compartment localization of interneuron (cytoplasm) and NeuN (nuclei) epitopes completely guarantee the correct non-overlapped visualization of both reactions and the interpretation of the results. Sections from different animals and ages were processed in parallel using same batches of solutions to minimize variability in immunolabelling conditions

Thioflavin-S staining

Free-floating sections were incubated for 5 minutes with 0.015% Thio-S (Sigma) in 50% ethanol, and then washed in 50% ethanol, in PBS, mounted onto gelatine-coated slides and coverslipped with 0.01M PBS containing 50% glycerin and 3% triethylenediamine.

Stereological analysis

.Immunopositive cells for SOM, NPY, PV or NeuN belonging to the different animal groups (WT, PS1 and PS1×APP) (*n*=5-6/age/group) were stereologically quantified (see [10;14]). Briefly, the quantitative analyses were performed using an Olympus BX61 microscope interfaced with a computer and a Olympus DP71 digital camera, and the NewCAST (Computer Assisted Stereological Toolbox) software package (Olympus, Denmark). Cell counting was done through the rostrocaudal extent of the lateral entorhinal cortex (between −2.06 mm anterior and -4.60 mm posterior to Bregman coordinates). Neurons were quantified in every seventh section (with a distance of 280μm), and an average of 7-8 sections was measured in each animal. Cortical boundaries were defined according a standard mouse stereotaxic brain atlas [18], in adjacent series of sections stained with cresyl violet. The cortical area was defined using a 4x objective and the number of neurons was counted using a 100x/1.35 objective. We used the optical 3 μm from de upper surfaces as look-up and those 3–13 μm from the surfaces as reference sections. The numerical density (ND; cells/mm^3) was estimated using the following formula: $ND=\sum Q^-/(\sum a \times h)$, where Q^- is the number of dissector-counted somatic profiles, a is the area of the counting frame (1874.2 μm^2) and h is the height of the optical dissector (10 μm). The precision of the individual estimations is expressed by the coefficient of error (CE) [20] using the following formula: $CE=1/Qx(3A-4B+C/12)^{1/2}$, where $A=\sum Q_i^2$, $B=\sum Q_i x Q_{i+1}$, $C=\sum Q_i x Q_{i+2}$. The CEs ranged between 0.07 and 0.1. An investigator who was blind to the experimental conditions (age, genotype and marker) performed neuronal profile counting.

Entorhinal cortex volume

We estimated the LEnt volume of WT (*n*=6) and PS1×APP mice (*n*=6) applying the Cavalieri's principle in combination with point counting. This method provides efficient and unbiased volume estimation: $V = a(p) \times d \times \sum Pi$, where '$a(p)$' is the area associated with each sampling point, 'd' the mean distance between two consecutively studied sections and '$\sum Pi$' is the sum of points hitting. From the complete rostrocaudal set of sections in each animal a 1:7 series was selected for analysis. An average of 7-8 sections was measured in each animal. The CEs of the volume were <0.07. Data demonstrated the absence of differences between WT, PS1 and PS1×APP mice at 6 months of age.

Plaque loading quantification

Thioflavine-S staining was observed under an Olympus BX-61 epifluorescent microscope using FITC filter and 4x objective. Images were acquired with an Olympus DP71 high-resolution digital camera using the Cell-A program. The camera settings were adjusted at the start of the experiment and maintained for uniformity. Digital images (4 sections/mouse) from 4 and 6-month-old PS1xAPP mice (n=4/age) were analyzed using Visilog 6.3 analysis program (Noesis, France). The plaque area (Thioflavin-S positive) within the entorhinal cortex was identified by level threshold which was maintained throughout the experiment for uniformity. The color images were converted to binary images with plaque and entorhinal cortex layers identified (superficial layers, from I to III; and deep layers, from IV to VI).

The cortical area in each 4x image was manually outlined. The plaque loading (%) for each tg mouse was estimated and defined as (sum plaque area measured/sum cortical area analyzed) x 100. The sums were taken over all slides sampled and a single plaque burden was computed for each mouse. The mean and standard deviation (SD) of the plaque loading were determined using all the available data. Quantitative comparisons were carried out on sections processed at the same time with same batches of solutions.

Plaque size morphometric analysis

Four coronal sections stained with Thioflavin-S from 4 (n=5) and 6-month old (n=5) PS1xAPP mice were analyzed using the nucleator method with isotropic probes by the NewCAST software package from Olympus stereological system. Deep entorhinal layers were analyzed using a counting frame of 7528.5 μm^2 and step length of 194.02x194.02 µm. For individual plaque measurement a 40x objective was used. Number of plaques/mm^2 falling into four surface categories (ranging from <200 μm^2 to >2000 μm^2) was calculated. Each analysis was done by a single examiner blinded to sample identities.

Statistical analysis

Data was expressed as mean ± S.D. The comparison between two mice groups (WT and PS1xAPP mice or PS1 and PS1xAPP tg mice) was done by two-tailed *t*-test, and for comparing several groups (WT, PS1 and PS1xAPP mice) and ages we used one-way ANOVA, followed by Tukey post-hoc multiple comparison test (SigmaStat® 2.03, SPSS Inc). For both test, the significance was set at 95% of confidence.

RESULTS

The number of SOM and NPY positive interneurons was selectively reduced in the entorhinal cortex of PS1xAPP at 6 months of age

We have previously reported that hippocampal dendritic inhibitory SOM/NPY interneurons (OL-M and HIPP cells) were severely affected, whereas PV interneurons were highly resistant in this AD model [10].

Thus, we have first analyzed the possible vulnerability of these interneuronal subsets in the entorhinal cortex, a brain region that is specifically damaged at early stages of this pathology. We have combined specific immunohistochemical detection of SOM and NPY interneurons with unbiased stereological cell counting method, in PS1xAPP, PS1 and WT mice at early ages (2, 4 and 6 month-old). SOM-positive non-pyramidal somata were found in cortical layers II-VI of entorhinal cortex (Fig. 1A, a1) and showed multipolar morphology with several primary dendritic processes immunolabeled (Fig. 1A, a3). These SOM-positive cells have profuse axonal arborisation throughout cortical layers I to IV, being denser in layer I. Qualitative assessment of PS1xAPP mice immunolabeled sections indicated a robust loss of SOM-positive cells at 6 months of age (Fig. 1A, a2), when compared to the age-matched WT (Fig. 1A, a1) or PS1 mice (not shown). In addition, the morphological examination showed the presence of numerous SOM-positive dystrophic neurites in the double tg mice, many of them associated to Aβ plaques (Fig. 1A, a4). However, no aberrant neurites were detected in PS1 tg mice (not shown) or control group (Fig. 1A, a1 and a3). The stereological study (Fig. 1B) demonstrated a significant decrease (56.20±8.09%, n=6; Tukey $p<0.001$) in the

numerical density (neurones/mm^3) of SOM-positive cells in PS1xAPP mice at 6 months of age. PS1 group did not showed changes.

In order to determine if there was a preferential lamina selective neuronal loss, we have also stereologically counted this GABAergic population in the superficial (I-III) and deep (IV-VI) layers of same 6-month-old PS1xAPP and WT groups. Data demonstrated the existence of homogeneous reduction of SOM-positive cell density through cortical laminae (51.51±17.30% in the superficial layers *vs* 51.16±19.42% in the deep layers; n=6, two tailed t-test $p \leq 0.005$). Furthermore, we found a parallel decrease in the SOM and VGAT mRNA expression, as assessed by quantitative real time RT-PCR (qPCR) from laser microdissected samples (-26.11±13.53%, n=4, Tukey $p<0.05$ and -34.23±21.33%, n=4, Tukey $p<0.05$, for SOM and VGAT, respectively).

It could be argued that the observed decrease in the SOM cell density was widespread through the CNS in this particular PS1xAPP model and irrelevant to the Aβ pathology. Thus, we have also quantified this intereneuron population in the auditory cortex, a neocortical region less affected by Aβ pathology (not shown) and in the striatum (non Aβ plaques) of the same 6 month-old PS1xAPP mice population. In the auditory cortex we observed a lower decrease of 34.59±7.91% (n=3; two tailed t-test $p<0.05$) whereas no significant changes were detected in striatal SOM interneurons, as compared with age-matched control mice. The reduction in the hippocampus for these inhibitory cells was between 50-60%, being CA1 and dentate gyrus the most affected areas [10]. Therefore, SOM-positive cells are preferentially affected in regions (hippocampus and entorhinal cortex) showing a profuse Aβ pathology and also severely affected in AD patients.

In the hippocampus of this model, the most damaged SOM population also co-expressed NPY neuropeptide [10]. Extensive co-localization of SOM and NPY was also reported in the cerebral cortex [21-25], Therefore, we also analyzed the NPY-positive population by immunohistochemistry. As shown (Fig. 1A, a5-a8), NPY-immunoreactivity was present in non-pyramidal cell bodies and fibers in all layers of the entorhinal cortex. Neuronal somata were immunolabeled whereas proximal dendrites were usually weakly immunostained (see Fig. 1A, a7). The number of NPY-positive somata, observed in control animals, was clearly inferior when compared to SOM-positive somata (Fig. 1A, a5 vs a1). By qualitative assessment the entorhinal cortex of 6 month-old PS1xAPP mice contained less number of NPY-positive somata (Fig. 1A, a6) than WT animals (see Fig. 1A, a5). Moreover, these PS1xAPP mice showed numerous dystrophic NPY-positive neurites, most of them associated to amyloid deposits (Fig. 1A, a6 and a8). In agreement with this, double SOM/NPY immunofluorescence labeling showed that the subpopulation of SOM cells that coexpresses NPY was highly affected in the PS1xAPP mice (not shown).

Stereological analysis (Fig. 1C) demonstrated a significant reduction in the density (neurons/mm^3) of NPY-positive cells (46.36±14.17%, n=6; Tukey $p<0.05$) in PS1xAPP mice at early ages, similar to the reduction observed for SOM cells.

On the other hand, we did not find differences in the numerical density (neurons/mm^3) of PV-positive cells in PS1xAPP mice (Fig. 1D) neither in the expression of PV mRNA by RT-PCR (not shown). All together, these findings indicated that, in this AD model, the SOM and NPY-positive entorhinal

interneurons, but not PV-cells, displayed an early vulnerability, as also observed in the hippocampal formation [10].

The number of principal cells was selectively decreased in the deep entorhinal layers of PS1xAPP at 6 months of age

We next examined whether the principal cell density was also affected at early ages in this PS1xAPP model. To specifically distinguish interneurons from principal cells, we have performed a multiple immunolabeling approach. The different molecular profiles of cortical interneurons can be defined by the combination of the interneuronal markers SOM, PV, CR and VIP [26]. Thus, to identify principal cells, we have first performed a multiple immunohistochemical labeling for bright field microscopy combining anti-SOM, anti-PV, anti-CR and anti-VIP antibodies (cytoplasm of all cortical interneuronal populations were labeled in dark blue color by using DAB-nickel as chromogen). This was followed by anti-NeuN to label all neuronal cells (nuclei appeared in light brown color by using only DAB as chromogen). With this experimental approach, 5x multiple immunohistochemical labeling, principal cells appeared as single NeuN-labeled whereas all interneurons displayed double labelling. We choose this approach to label all interneurons instead using classical GABA or GAD immunostaining because we have observed that the number of somata immunopositive for these markers (GABA and/or GAD) was always lower than for SOM or PV. This discrepancy could due to tissue antigen preservation, antibody penetration, intracellular location (cell body/axonal boutons), or simply that GABAergic neurons are not uniform with respect to level of GABA or GAD content to be detected by immunohistochemistry. Anyway, the appropriate

controls were performed to ensure methodological accuracy of the 5x multiple immunolabeling (see material and methods section). The single NeuN labelled neurons were then counted using unbiased stereological method in layers I-III (supragranular or superficial layers) and IV-VI (infragranular or deep layers) of the entorhinal cortex at 2- (before Aβ deposition) and 6- (moderate Aβ deposition and significant loss of SOM/NPY cells) months of age.

As shown in Fig. 2A (a1 and a2), at 2 months of age, the 5x immunolabeled sections displayed no qualitative differences between WT and PS1xAPP animals. However, at 6 months of age (Fig. 2C, c1 and c2), a marked decrease in the density of NeuN-labeled cells was clearly detected in PS1xAPP, as compared to WT littermates. This decrease was patent in the deep layers (Fig.2C, c3 and c4). Quantitative stereological study revealed, as expected, the absence of differences in principal cell counts (neurons/mm^3) between PS1xAPP and non-transgenic mice at 2 months of age (Fig. 2B). However, in 6-month-old tg mice a significant principal cell loss (compared to non-transgenic littermates) was detected (Fig. 2D). The cell loss (27.26±8.24%, n=6, 7-8 sections per animal, two tailed t-test, $p<0.001$) was concentrated, as predicted, in the infragranular layers whereas no significant differences were detected in supragranular layers. Though we have not analyzed layers V and VI separately, the degree of neuronal change seemed to be substantially larger in layer V than in layer VI. The early prominent principal neuronal loss in deep entorhinal layers highlights the selective vulnerability of these laminae in our model. This neuronal loss was not accompanied by a reduction of the entorhinal cortex volume (10.50±0.84, 9.98±0.93 or 9.93±1.52 mm^3, *n*=6, for WT, PS1 and PS1×APP respectively).

Taken together, these data demonstrated the existence of an early neurodegenerative process in the entorhinal cortex of this PS1xAPP model. This process specifically affected to SOM and/or NPY positive GABAergic cells and deep principal neurons. Most importantly, principal cell degeneration began early (6 months) in the entorhinal cortex and then proceeded later (18 months) in the hippocampus [10].

Entorhinal neurodegeneration in deep layers is associated with extracellular, rather than intracellular, Aβ accumulation

Based on the intracellular toxic effect of Aβ accumulation (see [27-30], the preferential diminution of the principal cell density in deep layers could be due to a preferential accumulation of these peptides in this particular brain region. Thus, we first investigated the Aβ plaque distribution using Thioflavin-S. As shown qualitatively in Fig. 3A, and quantitatively in Fig. 3B, the Aβ plaques were first detected in 4-month-old PS1xAPP mice. Furthermore, substantially more amyloid plaques were observed in the entorhinal cortex and hippocampus than in other brain areas (not shown), which reflects the early vulnerability of these two forebrain regions in this AD model as reported in humans [8;31;32].

To elucidate more fully the preferential spatial location of amyloid deposition, the area occupied by Thioflavin-S positive compact deposits were quantified in deep (IV-VI) and superficial (I-III) layers at 4 and 6 months of age. As shown, Fig. 3B, at 4 months of age, entorhinal amyloid load was 0.2±0.15% in superficial layers and 0.6±0.24% for deep layers. At 6 months, Aβ deposition rapidly increased reaching 0.9±0.65% and 3.9±1.14% loads in superficial and deep layers, respectively. Thus, Aβ load in deep layers was significantly greater

(3 times at 4 months and 4.3 times at 6 months, two tailed t-test $p<0.001$, n=4) than in superficial layers. Interestingly, the plaque formation in the deep layers was markedly accelerated during this two months period (amyloid burden was 6.5 times greater at 6 months than at 4 months, two tailed t-test $p<0.001$, n=4). The age-dependent increase in the total amyloid load in the deep layers appeared to be associated with both the number and the size of the plaques. To further support this observation, we have determined the number of plaques/mm^2 in the deep layers at 4 and 6 months of age. Plaques were dissected into four surface categories ranging from <200μm^2 to >2000μm^2 (Fig. 3C). As expected, there was a significant increase (2.5 times, n=5, two tailed t-test $p<0.05$) in the number of plaques/mm^2 at the age of 6 months (172.75±53.80 at 6 months vs 67.41±21.32 at 4 months). The number of plaques falling into the range of 200, 200-500 y 500-2000 μm2 increased (1.8, 2.3 and 11.3 times, respectively; n=5, two tailed t-test $p<0.05$) at 6 months of age compared to 4 months. Interestingly, the plaques within the range of 500-2000μm^2 displayed the highest increase.

These data were compatible with the existence of a preferential Aβ production in these entorhinal deep layers, as compared with superficial layers or other brain regions. Thus, we next investigated the expression of APP and its metabolites using the mAb 6E10. Immunostaining with 6E10 (Fig. 3D) revealed an extracellular Aβ accumulation similar to that observed using Thioflavin-S. On the other hand, intracellular 6E10 immunostaining was detectable since 2 months of age in numerous entorhinal neurons located in layers II, III and VI. Surprisingly, few scattered neurons in layer V displayed immunoreactivity for this antibody (see Fig. 3D, d1-3).

Because of 6E10 immunolabeled Aβ peptides as well as APP full length and C99 fragments, these data could indicate that layer V neurons did not express the APP. Thus, the presence or absence of intracellular APP in this particular entorhinal layer was further investigated using an anti-hAPP C-terminal antibody. For these experiments, we used 2-month-old PS1xAPP tg mice, an age well before the neuronal lost. In fact, double hAPP/6E10 immunofluorescent labeling revealed an overlapping of both markers within same neuronal somata (Fig. 4A, a1-a4). However, the double-immunostained neurons were predominantly located in superficial layers and in layer VI, whereas layer V was practically negative for both antibodies.

In order to confirm these findings, we have also used specific anti-Aβ1-40 and anti-Aβ1-42 antibodies in sections pre-treated with formic acid. As shown in Fig. 4B for Aβ42 no intraneuronal Aβ immunostaining was seen in the entorhinal cortex at early ages (2 and 4 months are shown in b1 and b2, respectively). As in other cortical layers, neurons in layer V were devoid of intracellular Aβ42 immunostaining (Fig. 4B, b4 and b5). However, other forebrain areas of same animals, such as motor cortex layer V neurons (Fig. 4B, b3 and b6) and subiculum (not shown), displayed marked intracellular Aβ42 labeling as early as 2 months of age. Therefore, our experimental approach (formic acid retrieval and anti-Aβ42 C-terminal specific antibody) was able to detect the intracellular Aβ. Interestingly, we have not found significant changes in the numerical density of layer V motor cortex neurons in 6 month-old PS1xAPP mice (167.92±27.44 $x10^3$ vs 188.02±60.36 $x10^3$ neurones/mm^3 for WT and PS1xAPP respectively; n=5).

Taken together, these data indicated that although a preferential accumulation of extracellular Aβ peptides seemed to occur in layer V and VI, the layer V principal cells did not express APP and, in consequence, could not accumulate intracellular Aβ peptides. Therefore, it is very unlikely that the layer V cell loss was induced by intracellular Aβ accumulation.

Early cytotoxic glial inflammatory response in the entorhinal cortex of PS1xAPP mice

The Aβ deposition was associated with a progressive activation of astro- and microglial cells [14;33]. However, the microglial activation could exhibit different phenotypes, such as alternative or classic, with different consequences in the neuronal survival. In this sense, the alternative phenotype could exert a neuroprotective role (by releasing IGF-1 or phagocyting Aβ peptides) whereas the classic phenotype produced and released potentially cytotoxic factors (such as TNF-alpha, TRAIL, FASL, NO) (see [14]). Thus, we have next characterized the inflammatory response in the entorhinal cortex of young (4-6 months old) WT, PS1 and PS1xAPP mice.

First, we have quantitatively determined the mRNA expression of key factors of the neuroinflammatory response, using qPCR in microdissected entorhinal cortex from 4 and 6 months of age (Fig. 5). As expected Fig. 5A), there was a significant up-regulation of the microglial marker CD11b (3.46±0.62, n=4; Tukey $p<0.001$) and astroglial marker GFAP (12.24±0.86, n=4; Tukey $p<0.001$) in 6 month-old PS1xAPP animals. The increase in GFAP mRNA in PS1xAPP tg mice was also significant at 4 months of age (2.22±0.67, n=4; Tukey $p=0.016$). Level of CD11b mRNA was also slightly elevated in 4 months

tg entorhinal cortex, although not reaching statistical significance. This early increase of CD11b and GFAP mRNAs correlated with the initial appearance of Aβ plaques.

We next analyzed the expression of several classic cytotoxic factors by qPCR. As shown (Fig. 5B), mRNA levels of TNF-alpha (2.60±0.97, n=4; Tukey $p<0.05$) and TRAIL (2.48±0.66, n=4; Tukey, $p<0.05$) were significant up-regulated in PS1xAPP mice since 4 months of age. The expression of TNF-alpha (4.77±2.62 n=4; Tukey $p<0.05$) further increased at 6 months of age and was accompanied by a concomitant significant increase in the death receptor TNFR1 mRNA (2.43±0.68, n=4; Tukey $p<0.05$). A high increase in FAS mRNA was detected as 6 months of age (3.99±1.37, n=4; Tukey $p<0.05$), whereas no changes were detected for FasL. In addition, the inducible form of NOS (iNOS) was also significantly increased (2.11±1.26, n=4; Tukey $p<0.05$) at 6 months of age. An upregulation of DR5 and Cox2 mRNAs was detected though it was not statistical significant (not shown). These data were consistent with the existence of an early (4-6 months), potentially cytotoxic, classic microglial response in the entorhinal cortex of PS1xAPP mice. We have also observed a similar microglial response in the hippocampus of PS1xAPP tg model [14]. However, this classic activation was delayed until relatively old ages (18 months). At 6 months of age, microglial activation in the hippocampus displayed an altenative phenotype, characterized by the absence of expression of cytotoxic factors. Thus, it seemed that the potential cytotoxic microglial response at the entorhinal cortex occurs very early in the life span of this model. In order to confirm this observation, we have directly compared the microglial response in hippocampal microdissected samples from the same 6 month-old animals. We have focused

our experiments in the stratus oriens, because this hippocampal area displayed a high extracellular Aβ deposition [10] As expected, the results, Fig. 5C, demonstrated the existence of a glial activation in PS1xAPP mice compared to age-matched WT animals, with a clear induction in the expression of CD11b (4.44±0.79, n=4, two tailed t-test $p<0.001$) and GFAP (10.53±2.85, n=4, two tailed t-test $p<0.001$) mRNAs. However, and also in consonance with our previous data, the expression of the classic toxic factors TNF-alpha, iNOS and FASL remained unaltered. In consequence, these results demonstrated the existence of an early (4-6 months) classic microglial activation restricted to, at least, the enthorinal cortex.

We then addressed the inflammatory response at the cellular level by immunohistochemistry. For this purpose, we have used anti-CD11b (Fig. 6A, a1 and a2) and anti-GFAP (Fig. 6B, b1 and b2) antibodies to identify activated microglial and astroglial cells respectively. Microscopic analysis demonstrated the presence of activated microglial cells surrounding Aβ plaques at 4 (not shown) and 6 months of age (Fig. 6A, a2). Most activated microglial cells were obviously found in deep layers where Aβ plaques concentrated. Morphologically, these activated glial cells displayed enlargement of the cell body and retraction and swelling of microglial processes (see inset of Fig. 6A, a2 and Fig. 6C, c7). Resting microglial showed small cell body and thin and highly ramified processes as seen in control mice (Fig. 6A, a1 and Fig. 6C, c8). GFAP immunostaining was also highly increased in PS1xAPP entorhinal cortex since early ages (Fig. 6B, b2) as compared to age-matched non-transgenic mice (Fig. 6B, b1). However, reactive astrocytes did not displayed a clear association with Aβ plaques, instead they were located along the cortical

column (see inset Fig. 6B, b2). The close association of activated microglia and plaques in double tg mice was confirmed by double fluorescent 6E10-Tomato lectin staining and confocal microscopy (supplemental Fig. 1, A1-A3). The microglial cells closely associated to plaques expressed YM-1 (supplemental Fig. 1, B1-B4), a marker of the non-proinflammatory alternative phenotype [34].

In the hippocampus of aged PS1xAPP mice inter-plaque microglial cells displayed an activated morphology and were YM-1 negative and TNF-alpha positive [14]. Thus, we have next determined the morphological activation of inter-plaque microglial cells in the entorhinal cortex of young PS1xAPP mice. For these particular experiments, we used anti-Iba1 antibody (another microglial marker) that allowed a better discrimination of the microglial morphological phenotype (compare Fig. 6A and 6C). As shown (Fig. 6C, c1 and c5), in 2-month-old PS1xAPP mice, no microglial activation was observed (Fig.6C, c4). In 4-month-old, most of the activated microglia was exclusively surrounded the Aβ plaques (stained with Congo red; Fig. 6C, c2). Most inter-plaque microglial cells appeared quiescent at this age (Fig. 6C, c6). However, in 6-month-old PS1xAPP mice, both the plaque-associated and inter-plaque microglial cells displayed a typical activated morphology (Fig.6, c6). These data indicated that, similar to 18-month-old hippocampus, the inter-plaque microglial cells in the entorhinal cortex of young transgenic mice were activated. Furthermore, the activated inter-plaque microglial cells were preferentially, although no exclusively, located in the deep layers of the entorhinal cortex.

Finally, we have also determined the cellular expression of two key potentially cytotoxic factors, TNF-alpha and iNOS, in the entorhinal cortex of PS1xAPP mice (Fig. 7). Concerning to TNF-alpha, results demonstrated an

intense and diffuse (probably due to soluble TNFalpha) immunostaining along the cortical column in 6-month-old PS1xAPP animals (Fig. 7A, a2), whereas age-matched control mice showed no immunoreactivity for this antigen (Fig. 7A, a1). No neuronal profiles were positive for TNF-alpha, instead immunoreactive cells with microglial morphology were observed (Fig. 7A, a3 and a4). Interestingly, the periphery of amyloid plaques, where numerous activated microglial cells were located, was immunonegative for this marker (Fig. 7A, a3). Thus, similar to that observed in hippocampus [14], microglial cells closely associated to deposits displayed a non cytotoxic TNF-negative (and YM-1 positive) phenotype. However, the inter-plaque microglia adopted a pro-inflammatory cytotoxic TNF-alpha positive (and YM1 negative) phenotype [14]. On the other hand, iNOS immunostaining was present in glial cells with astrocytic morphology since 4 months of age (Fig. 7B). At this early age these iNOS-positive cells were mainly located in the deep layers Fig. 7B, b2) whereas, at 6 months, they were also observed in superficial layers (Fig. 7B, b3). Double GFAP-iNOS labeling and confocal microscopy demonstrated the astrocytic origin of all iNOS-positive cells (Fig. 7C c1-c3). At 2 months of age, no iNOS-positive cells were detected in PS1xAPP (Fig. 7B, b1). Control mice showed none or very few iNOS positive cells at these early ages (Fig. 7B, b4).

DISCUSSION

The present study demonstrated: 1) early (6-months) significant neurodegeneration of principal cells, as well as SOM- and NPY-interneurons, in the entorhinal cortex of $PS1^{M146L}$xAPP^{751SL} transgenic mice; 2) principal cell loss occurred in deep layers while SOM cells were vulnerable along the cortical column; 3) selective entorhinal neurodegeneration was not associated with intracellular accumulation of Aβ instead coincided, spatial and temporally, with extracellular amyloid load and gliosis; importantly, this early glial inflammatory response exhibited a cytotoxic profile; 4) in the hippocampus, at the same age, the extracellular Aβ induced a non cytotoxic glial activation.

Though significant neuronal loss is a key feature in AD brains, most transgenic models for this pathology failed to undergo neurodegeneration, at least at early ages. We have previously demonstrated a significant (50-60%) early (6 months) loss of SOM/NPY interneurons in the hippocampus of this PS1xAPP model [10]. Here, we extend our previous finding and demonstrate that this dendritic inhibitory population was also preferentially affected (46-56%) in the entorhinal cortex. However, perisomatic PV interneurons were highly preserved [10]. These findings were strongly consistent with the prominent reduction of SOM and NPY neuropeptides in cortical post-mortem tissue from AD patients [35-42], that has been attributed to degeneration of intrinsic neurons [24;43-47].

On the other hand, while hippocampal pyramidal loss (30% in CA1) takes place at advanced ages (>17 months) in this model [13;14], our present results demonstrated a patent entorhinal principal cell loss in deep layers (27%) as

early as 6 months of age. To the best of our knowledge, this is the first report of such early and lamina selective neurodegeneration of entorhinal principal cells in an AD model. Our findings resemble the selective vulnerability of distinct types of principal neurons reported in AD patients [2;8;9]. Therefore, this PS1xAPP mouse could mimic the initial stages of the pathology in humans [2]; [9;48], showing temporal- and regional age-dependent vulnerability, with early entorhinal principal cell loss previous to hippocampal deterioration.

The molecular mechanism(s) that underlies this early entorhinal neuronal loss remains to be elucidated, however the Aβ peptides have been suggested as major contributors for neurodegeneration in AD (reviewed in [29;49;50]; see also [50]). In this sense, a correlation between intraneuronal Aβ and neuronal death/dysfunction has been described in several transgenic mice [27;30;51-53]. In our model, intracellular 6E10 immunostaining was found since very early ages (2 months), previous to the appearance of amyloid plaques [30;51;54;55]. However, and besides an intense intracellular immunoreactivity, no changes in the numerical density of layers II and III principal neurons were observed. On contrary, in layer V where pyramidal loss was concentrated, few scattered neuronal somata displayed 6E10 immunostaining, even in 2-month-old tg mice. Furthermore, few layer V neurons were also immunopositive for APP-C-terminal antibody at any age, indicating that most of the pyramidal neurons in this layer did not even express the transgenic hAPP. The monoclonal 6E10 could also recognize APP products, including full-length APP. Therefore, it is possible that the observed somatic 6E10 immunostaining corresponded, in fact, to the precursor proteins rather than Aβ (see Fig. 4A). Supporting this, we have not found intraneuronal immunoreactivity using either Aβ1-40 or Aβ1-42 antibodies

in any entorhinal layer (even using formic acid pre-treatment; see Fig 4B). However, robust intracellular Aβ1-42 immunoreactivity was indeed observed in motor cortex layer V neurons and in subicular neurons from the same animals.

In sum, although we do not know the reasons that determine the absence of expression of transgenic hAPP in layer V from this particular brain area (tg hAPPsl was clearly expressed by layer V principal cells in other cortical regions; not shown), it seems very unlikely that entorhinal neuronal death in our model resulted from intracellular Aβ pathology. In agreement with this idea, the selective loss of SOM/NPY cells was not either associated with intracellular amyloid accumulation since they do not express the mutated hAPP [10]. A recent study [56] in another PS1xAPP model has also found loss of neurons (monoaminergic -MAergic- cells from raphe nuclei) that was not associated with accumulation of intracellular Aβ. In fact, the loss of these neurons was preceded by MAergic axonal degeneration in forebrain areas that showed early Aβ deposits and glial (astroglial/microglial) reaction.

In the entorhinal cortex, also coincident with the amyloid plaque deposition, there was a marked glial activation. These activated microglial cells could exert a beneficial function, restricting plaque formation by phagocytosis, or promote disease by causing neuronal damage [10;14;57-59]. Moreover, microglia could display different phenotypes during disease progression (see Fig. 8). In fact, we have recently reported an age-dependent functional switch of microglial cells in the hippocampus of this model [14]. At early ages (6 months), hippocampal activated microglial cells were closely associated to amyloid deposits and displayed an alternative phenotype with neuroprotective features. On the other hand, at 18 months, hippocampal inter-plaque regions also

showed activated microglia though in this case with a classic cytotoxic phenotype (expressing TNF-alpha and related factors). The interplaque activation temporally correlated with marked hippocampal pyramidal loss. Similarly, entorhinal Aβ plaque-associated microglia displayed an alternative phenotype (YM1 positive, TNF-alpha negative). However, the inter-plaque microglia, at this early age, was already activated and displaying a classic, TNF-alpha positive, phenotype. Also in consonance with our previous data, a significant upregulation of TNFalpha, TRAIL as well as iNOs mRNAs was also observed at early ages. Furthermore, we have also observed a preferential expression of iNOS by reactive astrocytes located in deep entorhinal layers.

Based on these data, it is tempting to speculate that the early cytotoxic glial response (micro- and astroglial) observed in deep entorhinal layers might be implicated in the pyramidal cell loss at early ages. Thus, it is possible that this early inflammatory reaction might be also implicated in the degeneration of SOM cells in both deep and superficial layers. In fact, iNOs expression showed a clear temporal gradient from deep (at 4 months) to superficial layers (at 6 months), and TNF-alpha immunostaining was spread along the whole cortical column, probably due to diffusion of the soluble pool.

It is noteworthy that, using microdissected samples of hippocampal stratum oriens of the same mice population, we have confirmed the existence of a non-cytotoxic glial response at these early ages in the hippocampus (Fig. 5C and [14]). Therefore, it is relevant to consider that, at 6 months of age, the Aβ associated inflammatory response (see Fig. 8) could play different roles in entorhinal cortex (classic proinflammatory phenotype, probably involved in neurodegeneration) and hippocampus (alternative phenotype, probably

neuroprotective). The existence of opposite inflammatory reactions in the most vulnerable brain regions to AD, at the same chronological age, might be involved in the controversial/disappointing results of non-steroidal anti-inflammatory drugs trials for protecting against the development of AD [60;61].

At present, we do not know the nature of the Aβ species implicated in the microglial activation. However, soluble Aβ oligomers are reported to be the preferential toxic amyloid species [62-64]. Amyloid plaques are potentially major sources of soluble and toxic oligomeric Aβ [65]. Furthermore, we have recently reported microglial activation due to the oligomeric Aβ [14]. Thus, the preferential accumulation of Aβ plaques in deep layers (this paper), that agrees with the entorhinal connectivity and the synaptic release of Aβ, might also locally increase the concentration Aβ oligomers. This could, in consequence, induce a neuroinflammatory process that might substantially contribute to neurodegeneration by releasing cytotoxic agents [66-74]. We cannot discard a direct effect of such Aβ oligomers, affecting to the most vulnerable neuronal populations.

In sum, neurodegeneration of principal neurons in the entorhinal cortex of PS1xAPP model occurs earlier than in hippocampus, as also observed in AD brains. Furthermore, there is a profound early loss of SOM/NPY interneurons resembling also the neuropathology in humans. The ubiquitous loss of SOM cells seems to be correlated with the cytotoxic inflammatory reaction whereas the deep principal cells could be also affected by the preferential accumulation of extracellular Aβ. Therefore, simultaneously, during disease progression, the most vulnerable brain regions (entorhinal cortex and hippocampus) show different degree of pathology affectation and, more importantly, different

inflammatory profiles. In addition, these findings open the question of whether different neuronal subtypes (even within a single brain region) could display different vulnerability to several toxic environments, caused by the accumulation of Aβ species.

.

Acknowledgments: This work was supported by Spanish grants PI060556 (to AG), PI060567 (to JV), PI060781 (to DR) from Fondo de Investigación Sanitaria (FIS) -Instituto de Salud Carlos III-, and by Proyecto de Excelencia CVI-902 from Junta de Andalucia. IMG, DBV and SJ were the recipients of a contract from CIBERNED. MT and RSV held PhD fellowships from Junta de Andalucia and MEC of Spain, respectively.

References

[1] Braak H, Braak E (1997) Diagnostic criteria for neuropathologic assessment of Alzheimer's disease. *Neurobiol Aging* **18,** S85-S88

[2] Gomez-Isla T, Price JL, McKeel DW, Jr., Morris JC, Growdon JH, Hyman BT (1996) Profound loss of layer II entorhinal cortex neurons occurs in very mild Alzheimer's disease. *J Neurosci* **16,** 4491-4500

[3] Canto CB, Wouterlood FG, Witter MP (2008) What does the anatomical organization of the entorhinal cortex tell us? *Neural Plast* **2008,** 381243

[4] Chrobak JJ, Amaral DG (2007) Entorhinal cortex of the monkey: VII. intrinsic connections. *J Comp Neurol* **500,** 612-633

[5] Insausti R, Amaral DG (2008) Entorhinal cortex of the monkey: IV. Topographical and laminar organization of cortical afferents. *J Comp Neurol* **509,** 608-641

[6] Toledo-Morrell L, Stoub TR, Bulgakova M, Wilson RS, Bennett DA, Leurgans S, Wuu J, Turner DA (2004) MRI-derived entorhinal volume is a good predictor of conversion from MCI to AD. *Neurobiol Aging* **25,** 1197-1203

[7] Stoub TR, Toledo-Morrell L, Stebbins GT, Leurgans S, Bennett DA, Shah RC (2006) Hippocampal disconnection contributes to memory dysfunction in individuals at risk for Alzheimer's disease. *Proc Natl Acad Sci U S A* **103,** 10041-10045

[8] Braak H, Braak E (1991) Neuropathological stageing of Alzheimer-related changes. *Acta Neuropathol* **82,** 239-259

[9] Price JL, Ko AI, Wade MJ, Tsou SK, McKeel DW, Morris JC (2001) Neuron number in the entorhinal cortex and CA1 in preclinical Alzheimer disease. *Arch Neurol* **58,** 1395-1402

[10] Ramos B, Baglietto-Vargas D, Del Rio JC, Moreno-Gonzalez I, Santa-Maria C, Jimenez S, Caballero C, Lopez-Tellez JF, Khan ZU, Ruano D, Gutierrez A, Vitorica J (2006) Early neuropathology of somatostatin/NPY GABAergic cells in the hippocampus of a PS1xAPP transgenic model of Alzheimer's disease. *Neurobiol Aging* **27,** 1658-1672

[11] Blanchard V, Moussaoui S, Czech C, Touchet N, Bonici B, Planche M, Canton T, Jedidi I, Gohin M, Wirths O, Bayer TA, Langui D, Duyckaerts C, Tremp G, Pradier L (2003) Time sequence of maturation of dystrophic neurites associated with Abeta deposits in APP/PS1 transgenic mice. *Exp Neurol* **184,** 247-263

[12] Caballero C, Jimenez S, Moreno-Gonzalez I, Baglietto-Vargas D, Sanchez-Varo R, Gavilan MP, Ramos B, Del Rio JC, Vizuete M, Gutierrez A, Ruano D, Vitorica J (2007) Inter-individual variability in the expression of the mutated form of hPS1M146L determined the production of Abeta peptides in the PS1xAPP transgenic mice. *J Neurosci Res* **85,** 787-797

[13] Schmitz C, Rutten BP, Pielen A, Schafer S, Wirths O, Tremp G, Czech C, Blanchard V, Multhaup G, Rezaie P, Korr H, Steinbusch HW, Pradier L, Bayer TA (2004) Hippocampal neuron loss exceeds amyloid plaque load in a transgenic mouse model of Alzheimer's disease. *Am J Pathol* **164,** 1495-1502

[14] Jimenez S, Baglietto-Vargas D, Caballero C, Moreno-Gonzalez I, Torres M, Sanchez-Varo R, Ruano D, Vizuete M, Gutierrez A, Vitorica J (2008) Inflammatory

response in the hippocampus of PS1M146L/APP751SL mouse model of Alzheimer's disease: age-dependent switch in the microglial phenotype from alternative to classic. *J Neurosci* **28,** 11650-11661

[15] Colton CA, Mott RT, Sharpe H, Xu Q, Van Nostrand WE, Vitek MP (2006) Expression profiles for macrophage alternative activation genes in AD and in mouse models of AD. *J Neuroinflammation* **3,** 27

[16] van GT (2001) Entorhinal cortex of the mouse: cytoarchitectonical organization. *Hippocampus* **11,** 397-407

[17] Insausti R, Herrero MT, Witter MP (1997) Entorhinal cortex of the rat: cytoarchitectonic subdivisions and the origin and distribution of cortical efferents. *Hippocampus* **7,** 146-183

[18] Franklin K.B.J:Paxinos G (2008) *The mouse brain in stereotaxic coordinates*, Academic Press,

[19] Ruano D, Lambolez B, Rossier J, Paternain AV, Lerma J (1995) Kainate receptor subunits expressed in single cultured hippocampal neurons: molecular and functional variants by RNA editing. *Neuron* **14,** 1009-1017

[20] Gundersen HJ, Jensen EB, Kieu K, Nielsen J (1999) The efficiency of systematic sampling in stereology--reconsidered. *J Microsc* **193,** 199-211

[21] Vincent SR, Johansson O, Hokfelt T, Meyerson B, Sachs C, Elde RP, Terenius L, Kimmel J (1982) Neuropeptide coexistence in human cortical neurones. *Nature* **298,** 65-67

[22] Hendry SH, Jones EG, Emson PC (1984) Morphology, distribution, and synaptic relations of somatostatin- and neuropeptide Y-immunoreactive neurons in rat and monkey neocortex. *J Neurosci* **4,** 2497-2517

[23] Chronwall BM, Chase TN, O'Donohue TL (1984) Coexistence of neuropeptide Y and somatostatin in rat and human cortical and rat hypothalamic neurons. *Neurosci Lett* **52,** 213-217

[24] Chan-Palay V (1987) Somatostatin immunoreactive neurons in the human hippocampus and cortex shown by immunogold/silver intensification on vibratome sections: coexistence with neuropeptide Y neurons, and effects in Alzheimer-type dementia. *J Comp Neurol* **260,** 201-223

[25] Papadopoulos GC, Parnavelas JG, Cavanagh ME (1987) Extensive co-existence of neuropeptides in the rat visual cortex. *Brain Res* **420,** 95-99

[26] Miyoshi G, Butt SJ, Takebayashi H, Fishell G (2007) Physiologically distinct temporal cohorts of cortical interneurons arise from telencephalic Olig2-expressing precursors. *J Neurosci* **27,** 7786-7798

[27] Casas C, Sergeant N, Itier JM, Blanchard V, Wirths O, van der KN, Vingtdeux V, van de SE, Ret G, Canton T, Drobecq H, Clark A, Bonici B, Delacourte A, Benavides J, Schmitz C, Tremp G, Bayer TA, Benoit P, Pradier L (2004) Massive CA1/2 neuronal loss with intraneuronal and N-terminal truncated Abeta42 accumulation in a novel Alzheimer transgenic model. *Am J Pathol* **165,** 1289-1300

[28] Christensen DZ, Kraus SL, Flohr A, Cotel MC, Wirths O, Bayer TA (2008) Transient intraneuronal Abeta rather than extracellular plaque pathology correlates with neuron loss in the frontal cortex of APP/PS1KI mice. *Acta Neuropathol* **116,** 647-655

[29] Laferla FM, Green KN, Oddo S (2007) Intracellular amyloid-beta in Alzheimer's disease. *Nat Rev Neurosci* **8,** 499-509

[30] Oakley H, Cole SL, Logan S, Maus E, Shao P, Craft J, Guillozet-Bongaarts A, Ohno M, Disterhoft J, Van EL, Berry R, Vassar R (2006) Intraneuronal beta-amyloid aggregates, neurodegeneration, and neuron loss in transgenic mice with five familial Alzheimer's disease mutations: potential factors in amyloid plaque formation. *J Neurosci* **26,** 10129-10140

[31] Thal DR, Rub U, Schultz C, Sassin I, Ghebremedhin E, Del TK, Braak E, Braak H (2000) Sequence of Abeta-protein deposition in the human medial temporal lobe. *J Neuropathol Exp Neurol* **59,** 733-748

[32] Thal DR, Rub U, Orantes M, Braak H (2002) Phases of A beta-deposition in the human brain and its relevance for the development of AD. *Neurology* **58,** 1791-1800

[33] Bryan KJ, Zhu X, Harris PL, Perry G, Castellani RJ, Smith MA, Casadesus G (2008) Expression of CD74 is increased in neurofibrillary tangles in Alzheimer's disease. *Mol Neurodegener* **3,** 13

[34] Edwards MM, Robinson SR (2006) TNF alpha affects the expression of GFAP and S100B: implications for Alzheimer's disease. *J Neural Transm* **113,** 1709-1715

[35] Davies P, Katzman R, Terry RD (1980) Reduced somatostatin-like immunoreactivity in cerebral cortex from cases of Alzheimer disease and Alzheimer senile dementa. *Nature* **288,** 279-280

[36] Rossor MN, Emson PC, Mountjoy CQ, Roth M, Iversen LL (1980) Reduced amounts of immunoreactive somatostatin in the temporal cortex in senile dementia of Alzheimer type. *Neurosci Lett* **20,** 373-377

[37] Arai H, Moroji T, Kosaka K (1984) Somatostatin and vasoactive intestinal polypeptide in postmortem brains from patients with Alzheimer-type dementia. *Neurosci Lett* **52,** 73-78

[38] Beal MF, Mazurek MF, Svendsen CN, Bird ED, Martin JB (1986) Widespread reduction of somatostatin-like immunoreactivity in the cerebral cortex in Alzheimer's disease. *Ann Neurol* **20,** 489-495

[39] Beal MF, Mazurek MF, Chattha GK, Svendsen CN, Bird ED, Martin JB (1986) Neuropeptide Y immunoreactivity is reduced in cerebral cortex in Alzheimer's disease. *Ann Neurol* **20,** 282-288

[40] Reinikainen KJ, Riekkinen PJ, Jolkkonen J, Kosma VM, Soininen H (1987) Decreased somatostatin-like immunoreactivity in cerebral cortex and cerebrospinal fluid in Alzheimer's disease. *Brain Res* **402,** 103-108

[41] Grouselle D, Winsky-Sommerer R, David JP, Delacourte A, Dournaud P, Epelbaum J (1998) Loss of somatostatin-like immunoreactivity in the frontal cortex of Alzheimer patients carrying the apolipoprotein epsilon 4 allele. *Neurosci Lett* **255,** 21-24

[42] Davis KL, Mohs RC, Marin DB, Purohit DP, Perl DP, Lantz M, Austin G, Haroutunian V (1999) Neuropeptide abnormalities in patients with early Alzheimer disease. *Arch Gen Psychiatry* **56,** 981-987

[43] Morrison JH, Rogers J, Scherr S, Benoit R, Bloom FE (1985) Somatostatin immunoreactivity in neuritic plaques of Alzheimer's patients. *Nature* **314,** 90-92

[44] Beal MF, Benoit R, Mazurek MF, Bird ED, Martin JB (1986) Somatostatin-28(1-12)-like immunoreactivity is reduced in Alzheimer's disease cerebral cortex. *Brain Res* **368,** 380-383

[45] Nakamura S, Vincent SR (1986) Somatostatin- and neuropeptide Y-immunoreactive neurons in the neocortex in senile dementia of Alzheimer's type. *Brain Res* **370,** 11-20

[46] Gaspar P, Duyckaerts C, Febvret A, Benoit R, Beck B, Berger B (1989) Subpopulations of somatostatin 28-immunoreactive neurons display different vulnerability in senile dementia of the Alzheimer type. *Brain Res* **490,** 1-13

[47] Kumar U (2005) Expression of somatostatin receptor subtypes (SSTR1-5) in Alzheimer's disease brain: an immunohistochemical analysis. *Neuroscience* **134,** 525-538

[48] Kordower JH, Chu Y, Stebbins GT, DeKosky ST, Cochran EJ, Bennett D, Mufson EJ (2001) Loss and atrophy of layer II entorhinal cortex neurons in elderly people with mild cognitive impairment. *Ann Neurol* **49,** 202-213

[49] Li M, Chen L, Lee DH, Yu LC, Zhang Y (2007) The role of intracellular amyloid beta in Alzheimer's disease. *Prog Neurobiol* **83,** 131-139

[50] Castellani RJ, Zhu X, Lee HG, Moreira PI, Perry G, Smith MA (2007) Neuropathology and treatment of Alzheimer disease: did we lose the forest for the trees? *Expert Rev Neurother* **7,** 473-485

[51] Oddo S, Caccamo A, Shepherd JD, Murphy MP, Golde TE, Kayed R, Metherate R, Mattson MP, Akbari Y, Laferla FM (2003) Triple-transgenic model of Alzheimer's disease with plaques and tangles: intracellular Abeta and synaptic dysfunction. *Neuron* **39,** 409-421

[52] Billings LM, Oddo S, Green KN, McGaugh JL, Laferla FM (2005) Intraneuronal Abeta causes the onset of early Alzheimer's disease-related cognitive deficits in transgenic mice. *Neuron* **45,** 675-688

[53] Bayer TA, Wirths O (2008) [Alzheimer's disease : Molecular pathology, animal models, and current treatment.]. *Nervenarzt*

[54] Masliah E, Sisk A, Mallory M, Mucke L, Schenk D, Games D (1996) Comparison of neurodegenerative pathology in transgenic mice overexpressing V717F beta-amyloid precursor protein and Alzheimer's disease. *J Neurosci* **16,** 5795-5811

[55] Wirths O, Multhaup G, Czech C, Blanchard V, Moussaoui S, Tremp G, Pradier L, Beyreuther K, Bayer TA (2001) Intraneuronal Abeta accumulation precedes plaque formation in beta-amyloid precursor protein and presenilin-1 double-transgenic mice. *Neurosci Lett* **306,** 116-120

[56] Liu Y, Yoo MJ, Savonenko A, Stirling W, Price DL, Borchelt DR, Mamounas L, Lyons WE, Blue ME, Lee MK (2008) Amyloid pathology is associated with progressive monoaminergic neurodegeneration in a transgenic mouse model of Alzheimer's disease. *J Neurosci* **28,** 13805-13814

[57] Khoury JE, Luster AD (2008) Mechanisms of microglia accumulation in Alzheimer's disease: therapeutic implications. *Trends Pharmacol Sci*

[58] Farfara D, Lifshitz V, Frenkel D (2008) Neuroprotective and neurotoxic properties of glial cells in the pathogenesis of Alzheimer's disease. *J Cell Mol Med* **12,** 762-780

[59] Zhu X, Su B, Wang X, Smith MA, Perry G (2007) Causes of oxidative stress in Alzheimer disease. *Cell Mol Life Sci* **64,** 2202-2210

[60] McGeer PL, McGeer EG (2007) NSAIDs and Alzheimer disease: epidemiological, animal model and clinical studies. *Neurobiol Aging* **28,** 639-647

[61] Aisen PS (2008) The inflammatory hypothesis of Alzheimer disease: dead or alive? *Alzheimer Dis Assoc Disord* **22,** 4-5

[62] Lambert MP, Barlow AK, Chromy BA, Edwards C, Freed R, Liosatos M, Morgan TE, Rozovsky I, Trommer B, Viola KL, Wals P, Zhang C, Finch CE, Krafft GA, Klein WL (1998) Diffusible, nonfibrillar ligands derived from Abeta1-42 are potent central nervous system neurotoxins. *Proc Natl Acad Sci U S A* **95,** 6448-6453

[63] De Felice FG, Vieira MN, Saraiva LM, Figueroa-Villar JD, Garcia-Abreu J, Liu R, Chang L, Klein WL, Ferreira ST (2004) Targeting the neurotoxic species in Alzheimer's disease: inhibitors of Abeta oligomerization. *FASEB J* **18,** 1366-1372

[64] Haass C, Selkoe DJ (2007) Soluble protein oligomers in neurodegeneration: lessons from the Alzheimer's amyloid beta-peptide. *Nat Rev Mol Cell Biol* **8,** 101-112

[65] Martins IC, Kuperstein I, Wilkinson H, Maes E, Vanbrabant M, Jonckheere W, Van GP, Hartmann D, D'Hooge R, De SB, Schymkowitz J, Rousseau F (2008) Lipids revert inert Abeta amyloid fibrils to neurotoxic protofibrils that affect learning in mice. *EMBO J* **27,** 224-233

[66] Apelt J, Schliebs R (2001) Beta-amyloid-induced glial expression of both pro- and anti-inflammatory cytokines in cerebral cortex of aged transgenic Tg2576 mice with Alzheimer plaque pathology. *Brain Res* **894,** 21-30

[67] Chao CC, Hu S, Sheng WS, Bu D, Bukrinsky MI, Peterson PK (1996) Cytokine-stimulated astrocytes damage human neurons via a nitric oxide mechanism. *Glia* **16,** 276-284

[68] Craft JM, Watterson DM, Van Eldik LJ (2006) Human amyloid beta-induced neuroinflammation is an early event in neurodegeneration. *Glia* **53,** 484-490

[69] Hu J, Akama KT, Krafft GA, Chromy BA, Van Eldik LJ (1998) Amyloid-beta peptide activates cultured astrocytes: morphological alterations, cytokine induction and nitric oxide release. *Brain Res* **785,** 195-206

[70] Itagaki S, McGeer PL, Akiyama H, Zhu S, Selkoe D (1989) Relationship of microglia and astrocytes to amyloid deposits of Alzheimer disease. *J Neuroimmunol* **24,** 173-182

[71] Johnstone M, Gearing AJ, Miller KM (1999) A central role for astrocytes in the inflammatory response to beta-amyloid; chemokines, cytokines and reactive oxygen species are produced. *J Neuroimmunol* **93,** 182-193

[72] Mrak RE, Griffin WS (2005) Glia and their cytokines in progression of neurodegeneration. *Neurobiol Aging* **26,** 349-354

[73] Ralay RH, Craft JM, Hu W, Guo L, Wing LK, Van Eldik LJ, Watterson DM (2006) Glia as a therapeutic target: selective suppression of human amyloid-beta-

induced upregulation of brain proinflammatory cytokine production attenuates neurodegeneration. *J Neurosci* **26,** 662-670

[74] Zipp F, Aktas O (2006) The brain as a target of inflammation: common pathways link inflammatory and neurodegenerative diseases. *Trends Neurosci* **29,** 518-527

FIGURE LEGENDS

Figure 1. Selective loss of SOM and NPY cells in the entorhinal cortex of PS1xAPP mice at 6 months of age, A, Light microscopic images of SOM (a1-a4) and NPY (a5-a8) immunostaining in entorhinal sections of 6 month-old WT (a1 and a3 for SOM; a5 and a7 for NPY) and PS1xAPP (a2 and a4 for SOM; a6 and a8 for NPY) mice**.** The number of SOM and NPY somata (black arrows) was clearly reduced in PS1xAPP mice compared to age-matched WT. Abundant immunoreactive dystrophic neurites (white arrows) were seen in the double tg mice. **B-D,** Stereological quantification of SOM (B), NPY (C) and PV(D) positive cells in the entorhinal cortex of PS1xAPP, PS1 and WT mice at 2, 4 and 6 months of age. There was a significant decrease in the SOM and NPY neuronal densities (cells/mm^3) of PS1xAPP tg mice at 6 months of age. Data (mean±SD) were analyzed by one-way ANOVA (SOM $F(8,28)=4.95$, $p<0.001$; NPY $F(8,26=3.65$, $p=0.006$) followed by Tukey post-hoc multiple comparison test. *Significance ($p<0.05$) was indicated in the figure. No significant differences for PV-positive cell density were detected. n=6/age/group. Scale bars: a1, a2, a5 and a6, 100 µm; a3, a4, a7 and a8, 20 µm

Figure 2. Selective loss of principal cells in the deep layers of PS1xAPP entorhinal cortex at 6 months of age. Multiple 5X (SOM, PV, CR, VIP and NeuN)-immunolabeling in the entorhinal cortex of WT and PS1xAPP mice at 2 (**A**) and 6 months (**C**) of age. Principal cells (single labelled NeuN cells in brown) were immunohistochemically differentiated from interneurons

(SOM/PV/CR/VIP-labeled cells in dark blue). A noticeable decline of principal cells was found in PS1xAPP deep entorhinal layers at 6 months of age (c2) compared to age-matched controls (c1); see also higher magnification of layer V from 6 month-old PS1xAPP (c4) and WT (c3). No differences were found at 2 months of age (a2 vs a1). **B** and **D**, Stereological counts of principal cells in superficial (I-III) and deep (IV-VI) entorhinal layers from WT and PS1xAPP mice at 2 (B) and 6 (D) months of age. Data (mean±SD) revealed a significant decrease of principal cell density (neurones/mm3) in 6 month-old PS1xAPP deep layers (n=6, 7-8 sections per mouse, two tailed t-test, **p<0.001). No significant changes were detected in superficial layers. Scale bars: a1, a2, c1 and c2, 100 μm; c3 and c4, 50 μm.

Figure 3. Extracellular Aβ deposits are preferentially located in deep layers of entorhinal cortex in PSxAPP mice at early ages. A, Thioflavin-S staining in entorhinal cortex of PS1xAPP at 2 (a1), 4 (a2) and 6 (a3) months of age. Amyloid deposits were first seen at 4 months of age. No intracellular Thioflavin staining was detected at these ages. **B,** Entorhinal Aβ load was significantly higher in deep layers than in superficial layers (two tailed t-test **p<0.001, n=4) at 4 and 6 months of age. **C,** The number and the size of the plaques in deep layers exhibited a considerable and significant increase from 4 to 6 months of age (two tailed t-test *p<0.05, n=4). **D,** 6E10 immunostaining in the entorhinal cortex of PS1xAPP mice at 2 (d1), 4 (d2) and 6 (d3) months of age. Amyloid deposits were detected at 4 months and then increased at 6 months of age. Intracellular 6E10 immunostaining was seen since 2 months of

age in layers II, III and VI, whereas most neurons in layer V were immunonegative. Scale bars: a1-a3 and b1-b3, 100 μm;

Figure 4. Entorhinal neurons of PS1xAPP mice do not accumulate intracellular Aβ at early ages. A, Double 6E10(a1)/hAPP(a2) immunofluorescence labelling, together with nuclear DAPI (a3) counterstaining, in 2 month-old PS1xAPP entorhinal cortex**.** Merged image (a4) shows coincidence of 6E10 and APP immunostaining in same neuronal somata. None or very few neuronal bodies in layer V displayed immunoreactivity for these antibodies. Sections were examined under an epifluorescent Olympus BX-61 microscope. **B,** Sections from entorhinal (b1, b2, b4 and b5) and motor (b3 and b6) cortex of 2 (b1, b3, b4 and b6) and 4 (b2 and b5) month-old PS1xAPP mice immunolabeled with Aβ1-42 antibody (after formic acid pre-treatment) and counterstained with cresil violet. Aβ1-42 immunoreactivity was only found in amyloid plaques at 4 months of age (big arrows) and no intraneuronally, however neurons of layer V in motor cortex of same mice at 2 months of age displayed robust intracellular Aβ immunostaining. Small arrows in b4 and b5 point layer V entorhinal neurons devoid of intraneuronal Aβ, whereas in b6 arrows point layer V motor neurons with intracellular punctuate immunolabeling. Inset shows higher magnification of a layer V motor neuron that accumulates Aβ1-42. Scale bars: a1-a4 and b1-b3, 100 μm; b4-b6, 20 μm; inset in b6, 10 μm.

Figure 5. Early glial activation displays a cytotoxic profile in the entorhinal cortex and a non-cytotoxic profile in the hippocampal stratum oriens of PS1xAPP mice. The mRNA expression of several inflammatory markers was determined by qPCR in microdissected samples of entorhinal cortex (A and B) and hippocampal stratum oriens (C) from 4 (n=4) and 6 (n=4) month-old PS1xAPP mice. **A,** Significant increase of CD11b (microglia) and GFAP (astrocytes) mRNAs was detected at 6 months of age. GFAP mRNA was also significantly upregulated at 4 month of age. **B,** A significant increase of iNOS, TNFalpha, TNFR1, TRAIL and FASL was determined at 6 months of age. The expression of TNFR1 and TRAIL was also upregulated at 4 months of age. No changes were detected for FasL at 6 months. Data (mean±SD) were analyzed by one-way ANOVA (GFAP $F(2,12)=577,92$, $p<0.001$; CD11b $F(2,12)=61,62$, $p<0.001$; TNFalpha $F(2,10)=7,35$, $p=0.01$; TNFR1 $F(2,12)=11,75$, $p=0.001$; TRAIL $F(2,9)=15,81$, $p=0.001$; FAS $F(2,12)=11,58$, $p=0.002$; iNOS $F(2,11)=4,17$, $p=0.04$) followed by Tukey post-hoc multiple comparison test. Significance (**p<0.001; *p<0.05) was indicated in the figure. **C,** Significant increase in the mRNA expression of CD11b and GFAP was detected in the stratum oriens of PS1xAPP mice at 6 months of age. However, in this region there were no significant changes in the mRNA expression of iNOS, TNFalpha, Fas and FASL. Data (mean±SD) are expressed in reference to 6 months-old WT mice. Significant difference from age matched WT mice; two tailed t-test, **p<00.01, *p<0.05.

Figure 6. Cellular expression of microglial (CD11b and Iba-1) and astroglial (GFAP) markers in the entorhinal cortex of young PS1xAPP

mice. A, CD11b immunostaining shows resting microglial cells distributed throughout cortical laminae in WT mice (a1) and the presence of activated microglial cells, surrounding Aβ plaques (arrows), mainly located in deep layers in PS1xAPP (a2) at 6 months of age. Activated microglia is morphologically characterized by hypertrophic cell body and numerous short and thick processes (see inset in a2). **B,** GFAP immunohistochemistry revealed a remarkable astrogliosis in the double tg mice (b2) compared to control animals (b1). Higher magnification of a reactive astrocyte is shown in b2 inset. **C,** Iba-1 immunostaining highlighted microglial cell morphology allowing a clear indentification of activated microglia in PS1xAPP mice. At 4 months of age, most activated microglia was closely associated to Aβ plaque (c2, arrows) and very few could be seen in the inter-plaques regions (c6, white arrow point to a resident microglia while black arrow points to a slightly activated microglial cell). However at 6 months, besides Aβ plaques surrounding microglia (arrows) numerous inter-plaques microglial cells were also activated (c3 and c7). No microglia activation was seen in 2 month-old PS1xAPP (c1; c5 shows a resident microglia) neither in 6-month-old WT mice (c4; c8 shows a resident microglial cell). Scale bars: a1, a2, b1 and b2, c1-c4, 100 µm; Insets a2 and b2, 10 µm; c5-c8, 10 µm.

Figure 7. Cellular immunolocalization of TNFalpha and iNOS in the entorhinal cortex of 6 month-old PS1xAPP mice. A, Strong TNF-alpha immunoreactivity was observed widespread in all layers of the entorhinal cortex of PS1xAPP (a2) except in the periphery of Congo red stained Aβ plaques (a3). TNF-alpha-positive cells displayed clear microglial morphology (a4; and arrows

in a3). No immunostaining for TNFalpha was detected in WT animal (a1). **B,** iNOS immunostaining was found in astroglial-like cells mainly in deep entorhinal layers at 4 months of age in PS1xAPP (b2) and then spread to other cortical layers at 6 months of age (b3). Inset in b3 shows a higher magnification image of a iNOS-positive cell. No immunostaining was found in 2 month-old PS1xAPP (b1). Control mice entorhinal cortex was immunonegative for iNOS as shown here at 6 months of age (b4). **C,** Double immunofluorescence labelling and confocal microscopy revealed that iNOS immunoreactivity was specifically localized in GFAP-positive astroglial cells. Scale bars: a1 and a2, 100 μm; a3, 25 μm; a4, 10 μm; b1-b4, 100 μm; inset in b3, 20 μm; c1-c3, 10 μm

Figure 8. Schematic representation of the microglial activation by Aβ and its age-dependent neuroprotective or neurodegenerative effect in PS1xAPP entorrinal cortex and hippocampus. At 4 months of age in both regions, Aβ deposits promote microglial activation to an alternative phenotype (YM1-positive) that show phagocytic capability and expression of IGF1. At the same time, reactive astrocytes, recruited by Aβ, release IL-4 that induces differentation of microglial cells to an alternative stage. This alternative microglia, only surround Aβ plaques, might contribute to neuronal protection. However, at 6 months of age in the entorhinal cortex, and much later (18 months) in the hippocampus, extracellular Aβ (plaques and/or oligomeric soluble forms) induce the activation of interplaque microglial cells to a classical phenotype and release of cytotoxic molecules (TNFalpha, TRAIL, FASL) that are harmful for neurons. Reactive astrocytes (non-associated to plaques) probably contribute to neurodegeneration by NO-mediated neurotoxicity. Aβ

plaques might be a source of soluble oligomeric Aβ. Dashed lines indicate proposed mechanisms. EC, entorhinal cortex; Hp, hippocampus. See also [14],

Supplemental Figure 1. Activated microglial cells are closely associated to amyloid plaques and display an alternative phenotype. Tomato lectin (TL) /6E10 (A1-A3) double fluorescence labeling in 6 month-old PS1xAPP entorhinal cortex. Activated microglial cells (tomato lectin-positive) were mainly found surrounding and infiltrating Aβ plaques (6E10 immunopositive). B1, Puctuate immunostaining for the microglial alternative activation marker YM1 was found around plaques (asterisk). Some cellular bodies could be also identified (arrow). YM1/Tomato lectin double labelling (B2-B4) showed the presence of this marker in microglial cells. Confocal microscopy. Scale bars: A1-A3, 20 μm; B1, 25 μm; B2-B4, 5 μm.

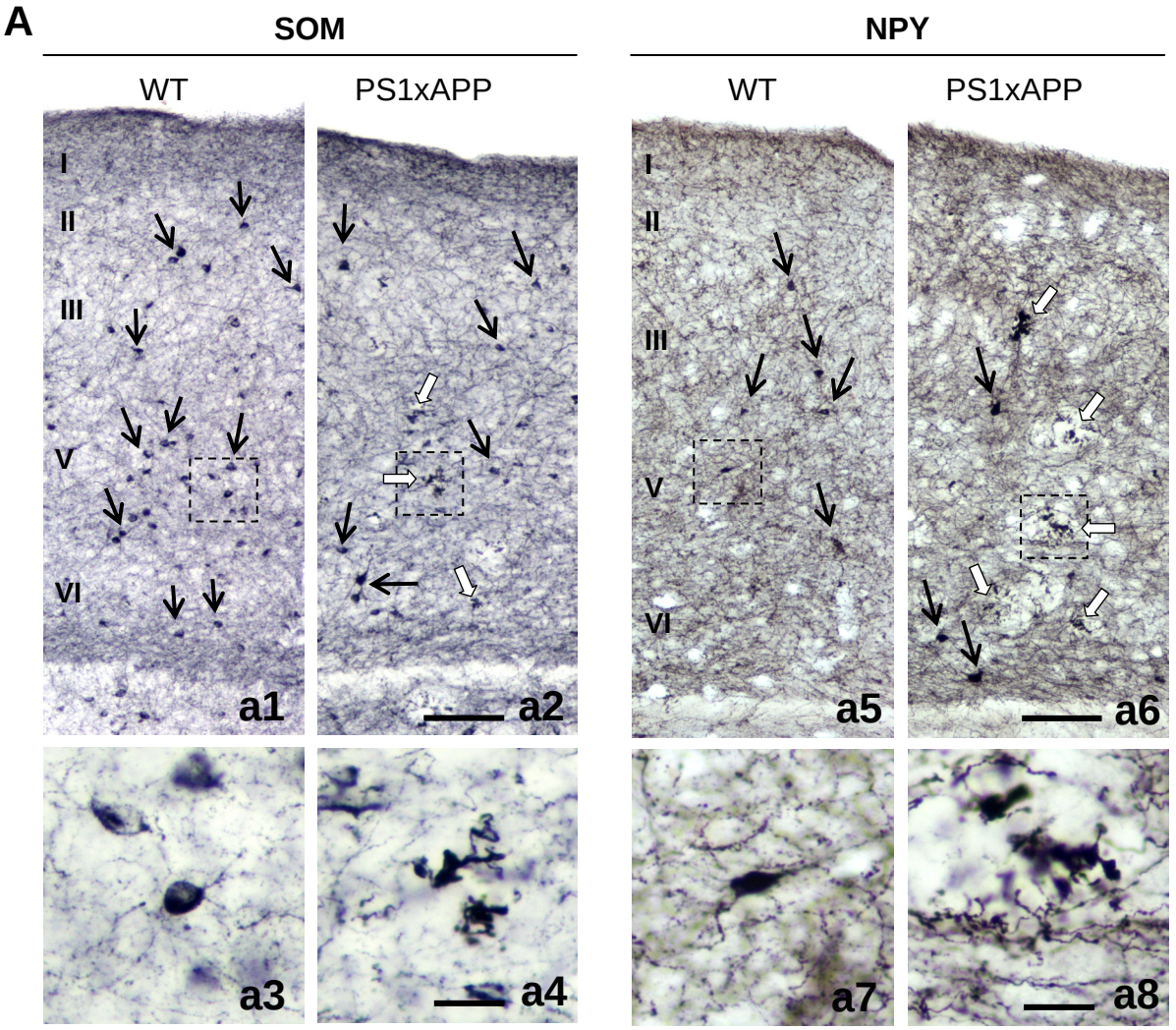
A
SOM
NPY
WT
PS1xAPP
WT
PS1xAPP
I
II
III
V
VI
a1
a2
a5
a6
a3
a4
a7
a8

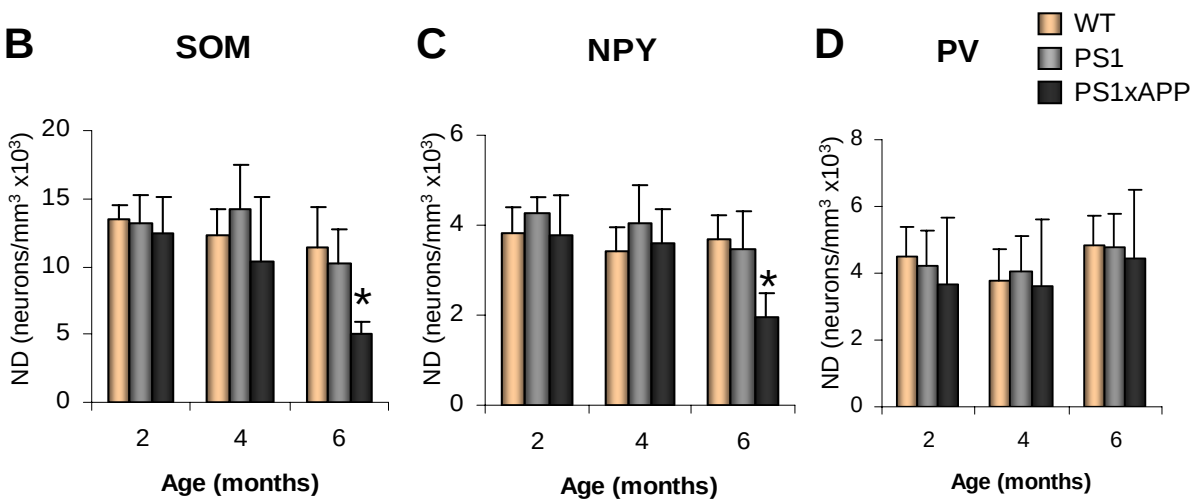
B
SOM
C
NPY
D
PV
WT
PS1
PS1xAPP
ND (neurons/mm3 x103)
Age (months)
2
4
6
0
5
10
15
20
*

Figure 1

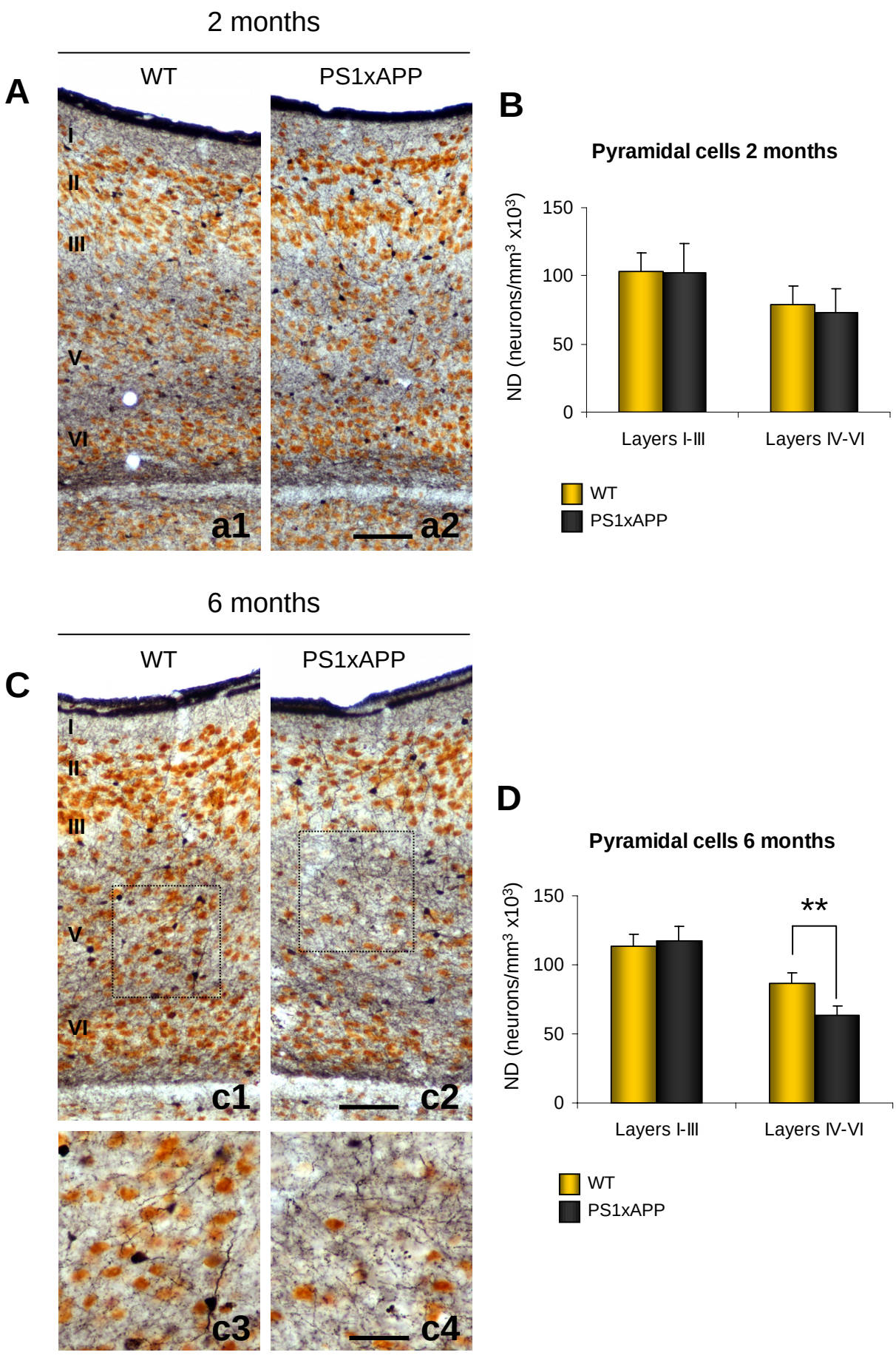
2 months
A
WT
PS1xAPP
I
II
III
V
VI
a1
a2
B
Pyramidal cells 2 months
ND (neurons/mm³ x10³)
150
100
50
0
Layers I-III
Layers IV-VI
WT
PS1xAPP
6 months
C
WT
PS1xAPP
I
II
III
V
VI
c1
c2
c3
c4
D
Pyramidal cells 6 months
ND (neurons/mm³ x10³)
150
100
50
0
**
Layers I-III
Layers IV-VI
WT
PS1xAPP

Figure 2

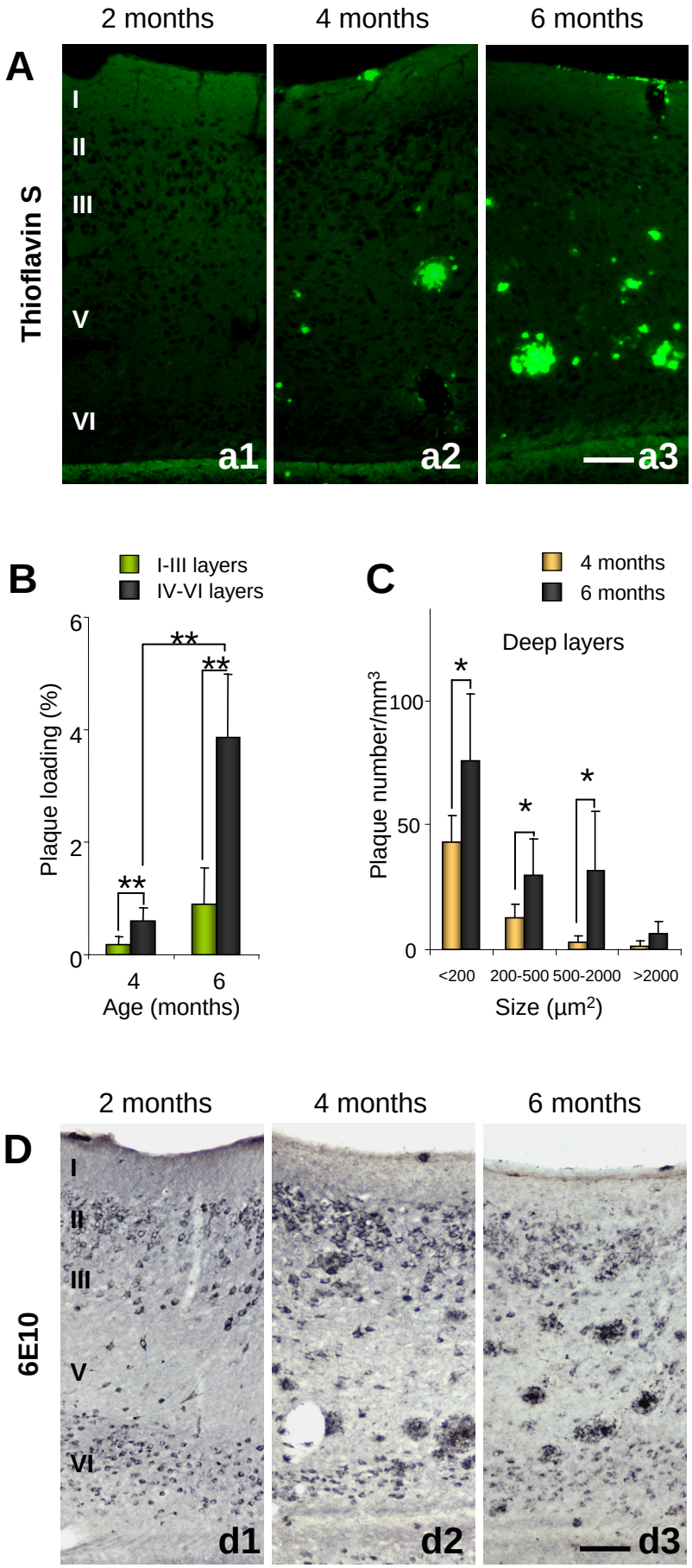
2 months
4 months
6 months
A
Thioflavin S
I
II
III
V
VI
a1
a2
a3
B
I-III layers
IV-VI layers
Plaque loading (%)
Age (months)
C
4 months
6 months
Deep layers
Plaque number/mm3
Size (µm2)
<200
200-500
500-2000
>2000
D
6E10
d1
d2
d3

Figure 3

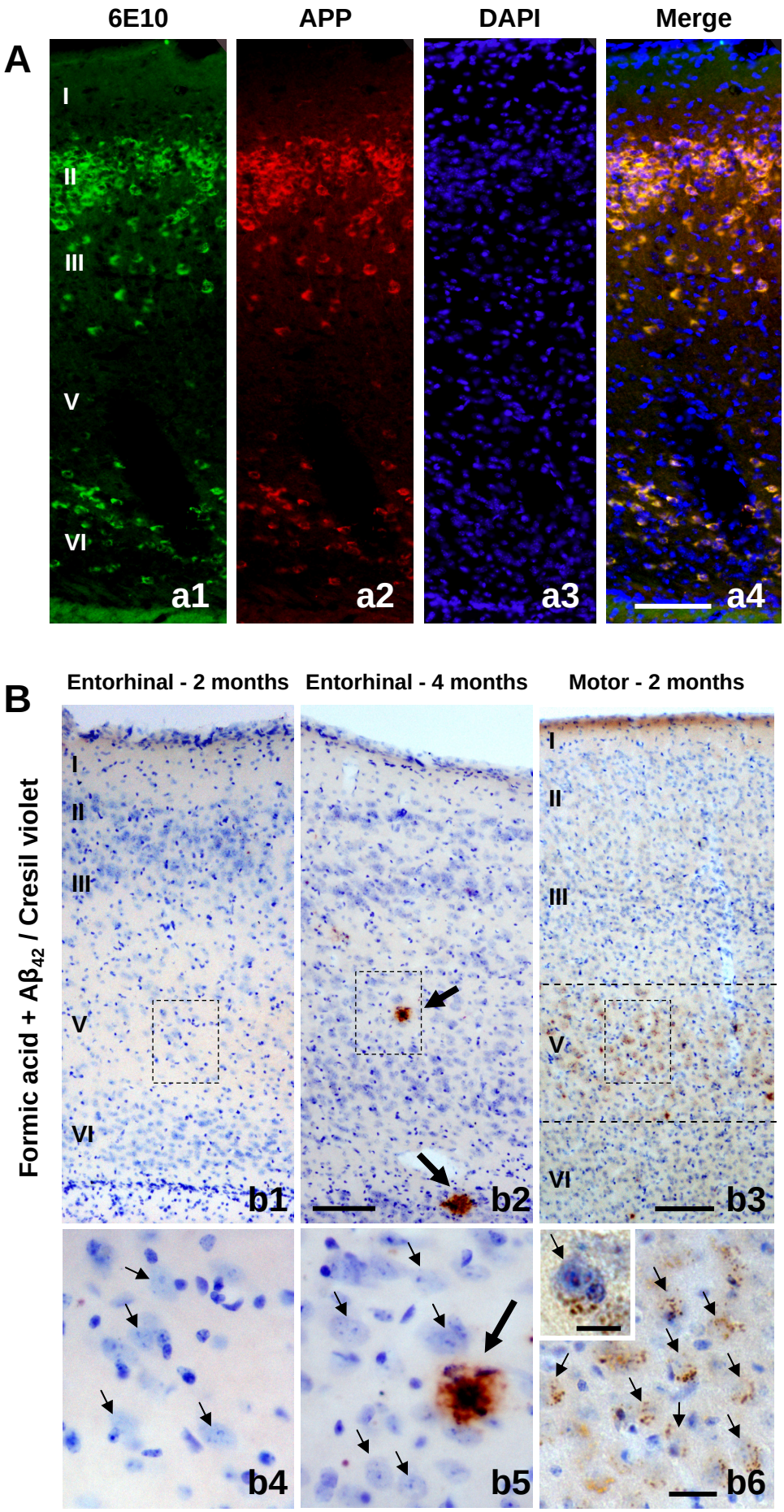
A
6E10
APP
DAPI
Merge
I
II
III
V
VI
a1
a2
a3
a4
B
Entorhinal - 2 months
Entorhinal - 4 months
Motor - 2 months
Formic acid + Aβ42 / Cresil violet
b1
b2
b3
b4
b5
b6

Figure 4

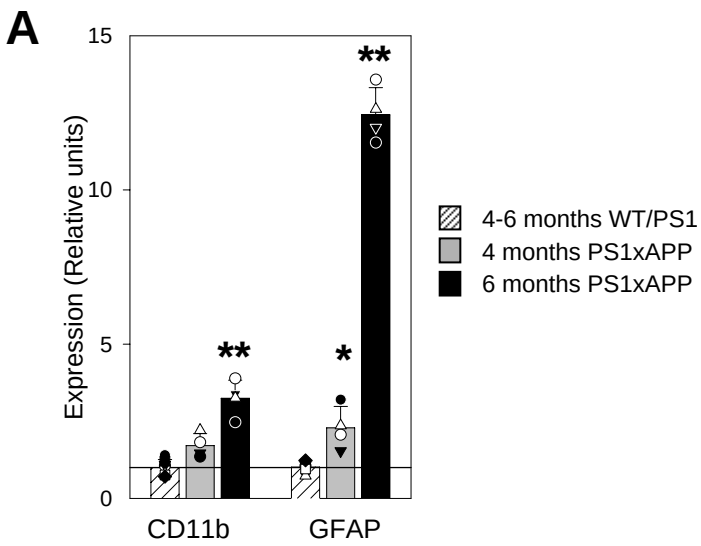
A
Expression (Relative units)
15
10
5
0
**
**
*
4-6 months WT/PS1
4 months PS1xAPP
6 months PS1xAPP
CD11b
GFAP

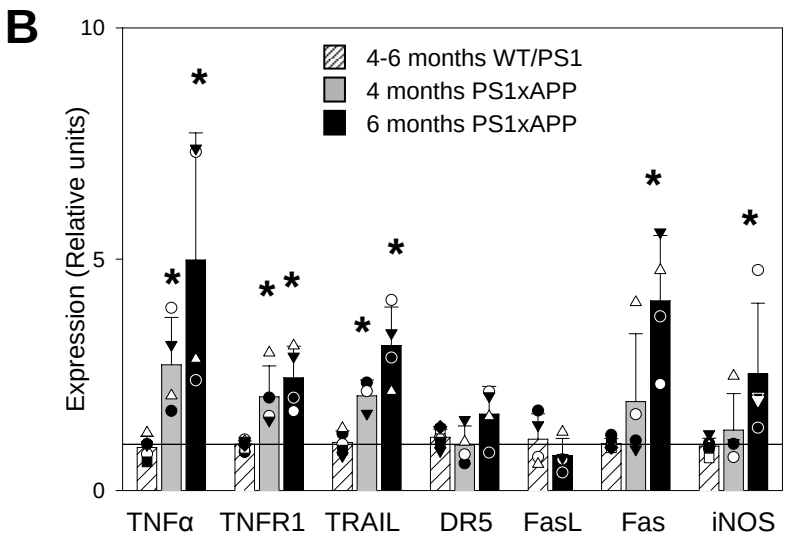
B
Expression (Relative units)
10
5
0
4-6 months WT/PS1
4 months PS1xAPP
6 months PS1xAPP
TNFα
TNFR1
TRAIL
DR5
FasL
Fas
iNOS

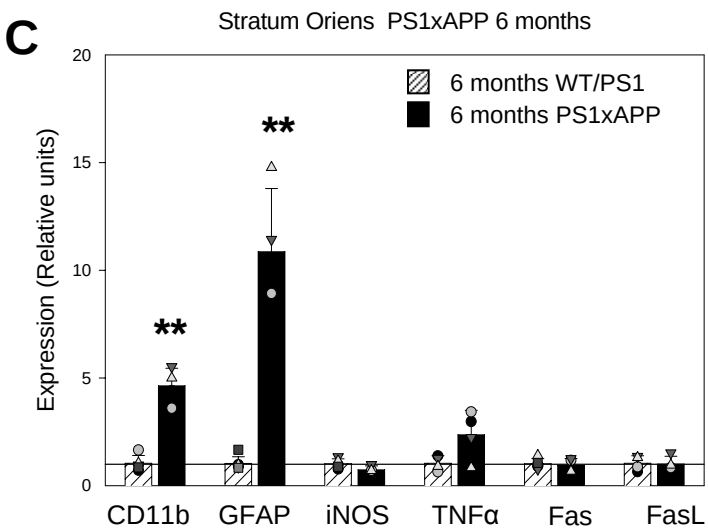
C
Stratum Oriens PS1xAPP 6 months
Expression (Relative units)
20
15
10
5
0
6 months WT/PS1
6 months PS1xAPP
**
**
CD11b
GFAP
iNOS
TNFα
Fas
FasL

Figure 5

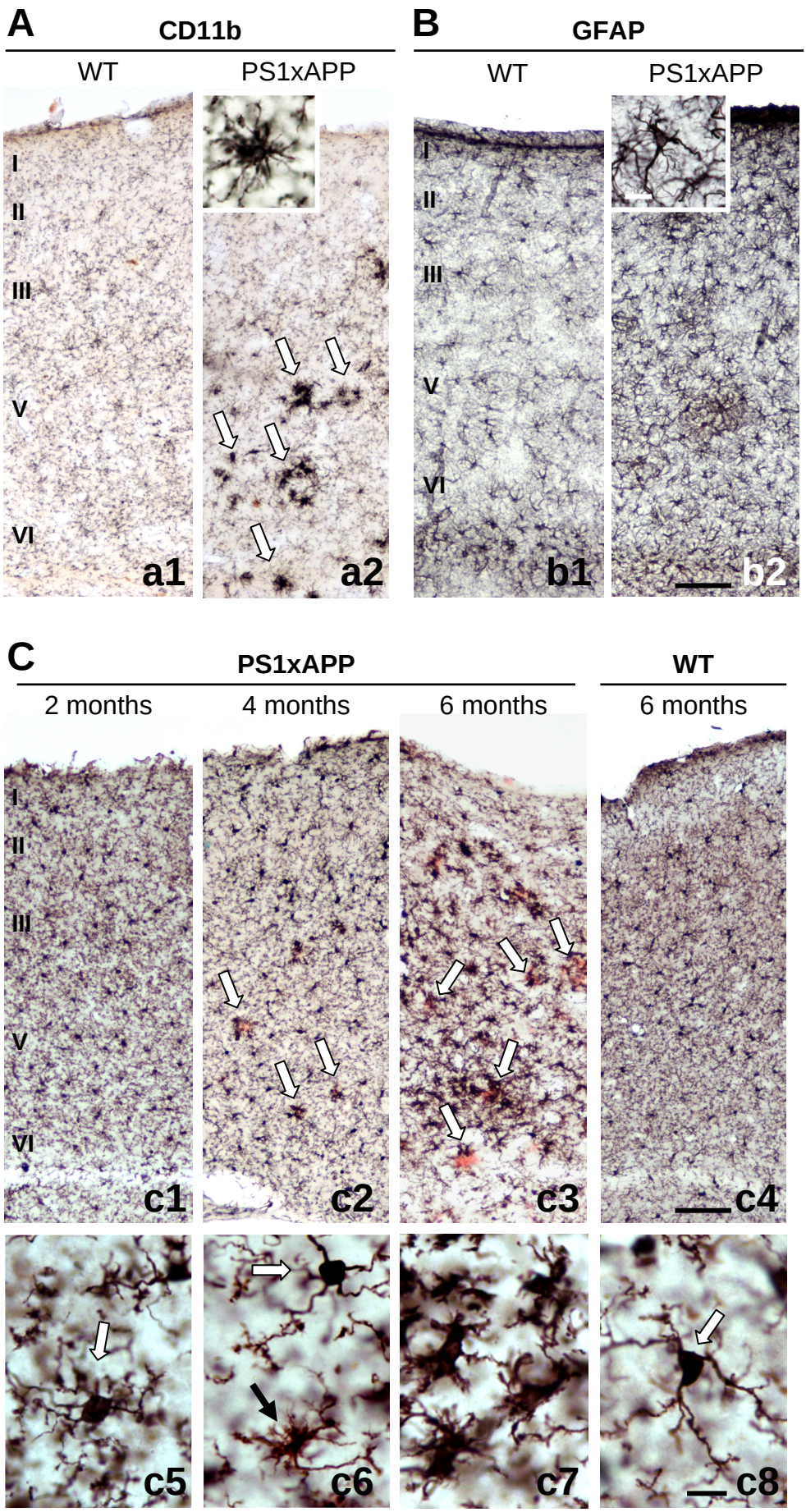
A
CD11b
WT
PS1xAPP
I
II
III
V
VI
a1
a2
B
GFAP
WT
PS1xAPP
I
II
III
V
VI
b1
b2
C
PS1xAPP
WT
2 months
4 months
6 months
6 months
I
II
III
V
VI
c1
c2
c3
c4
c5
c6
c7
c8

Figure 6

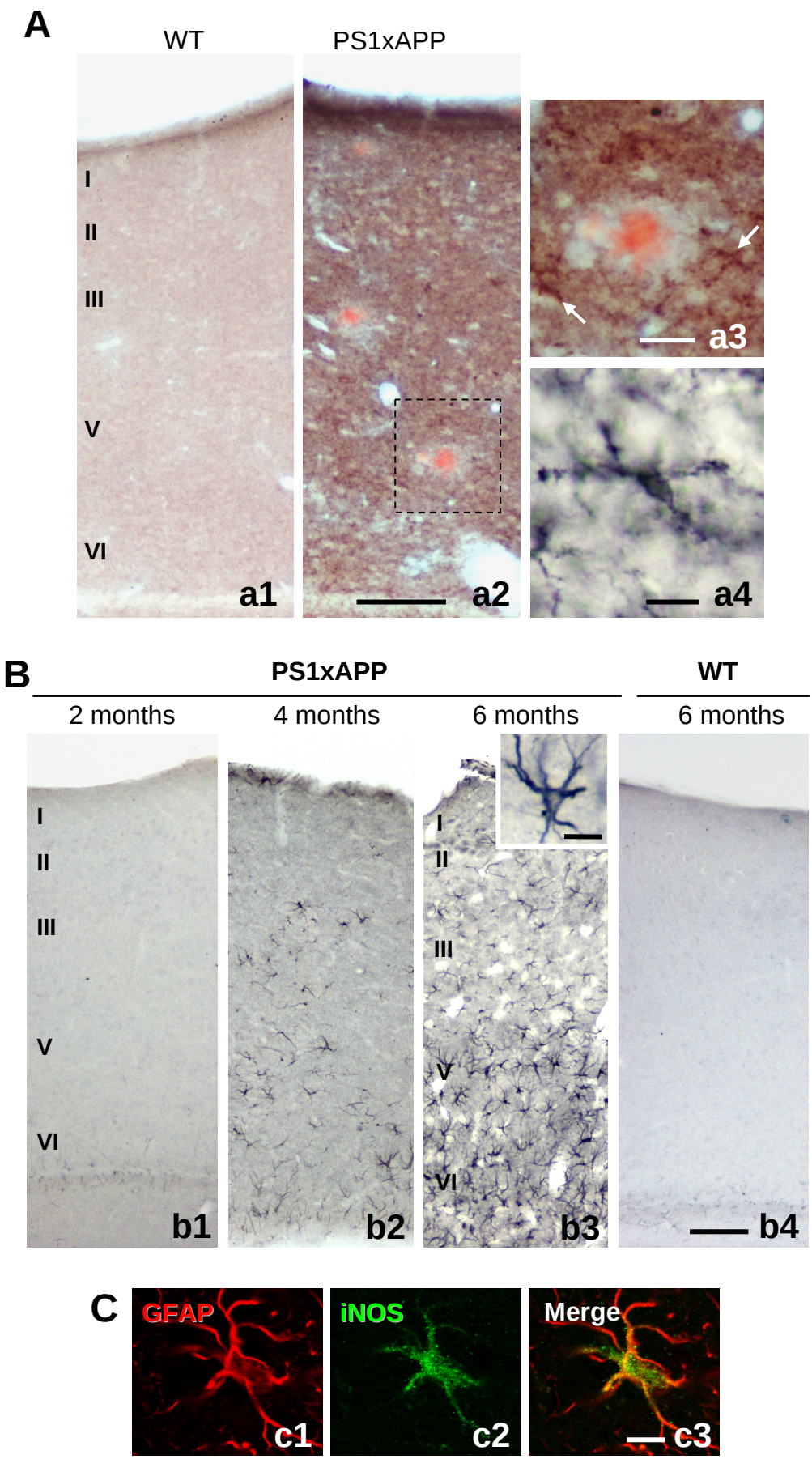
A
WT
PS1xAPP
I
II
III
V
VI
a1
a2
a3
a4
B
PS1xAPP
WT
2 months
4 months
6 months
6 months
I
II
III
V
VI
b1
b2
b3
b4
C
GFAP
iNOS
Merge
c1
c2
c3

Figure 7

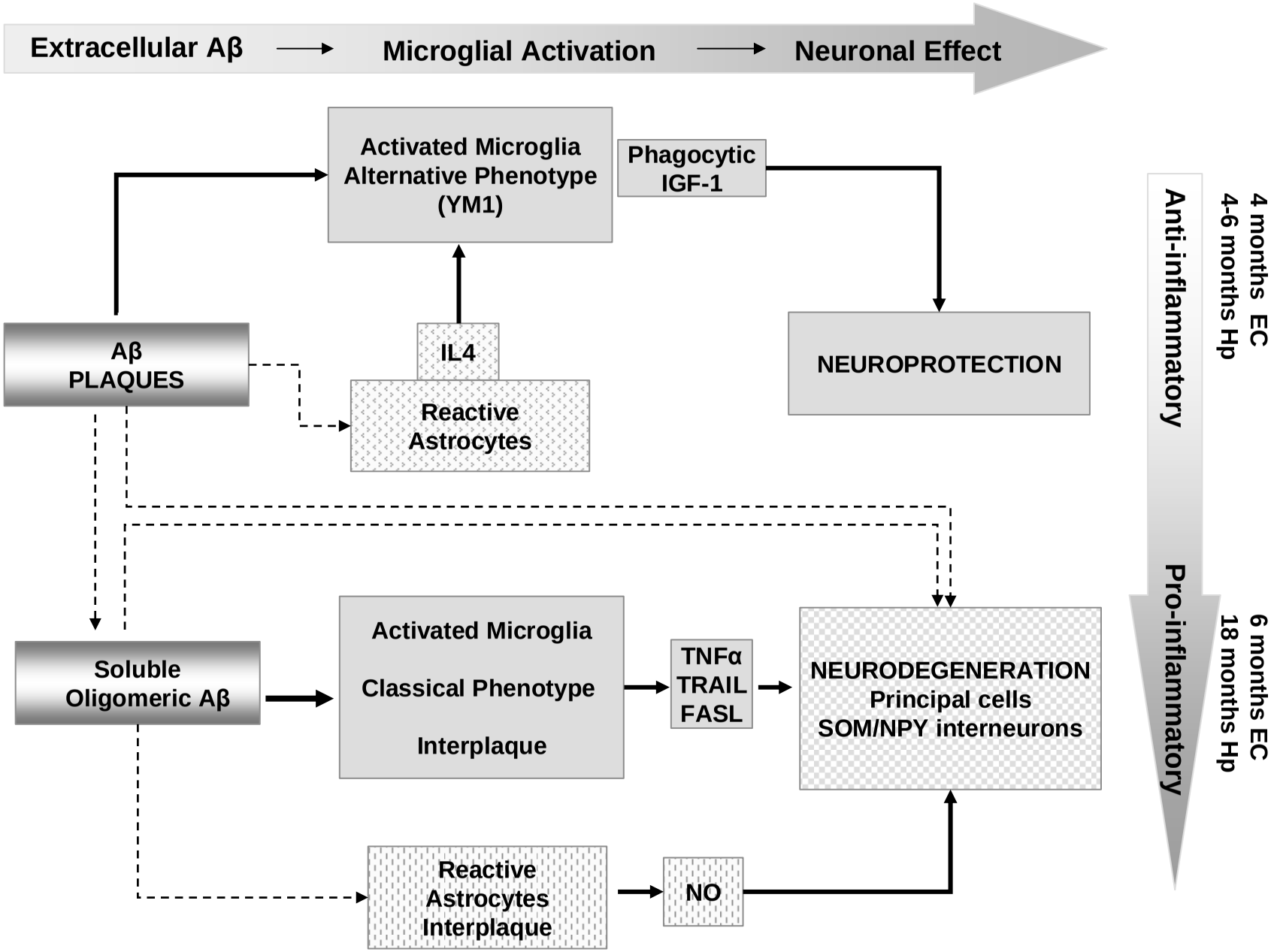
Extracellular Aβ
Microglial Activation
Neuronal Effect
Activated Microglia
Alternative Phenotype
(YM1)
Phagocytic
IGF-1
Aβ
PLAQUES
IL4
Reactive
Astrocytes
NEUROPROTECTION
Soluble
Oligomeric Aβ
Activated Microglia
Classical Phenotype
Interplaque
TNFα
TRAIL
FASL
NEURODEGENERATION
Principal cells
SOM/NPY interneurons
Reactive
Astrocytes
Interplaque
NO
Anti-inflammatory
Pro-inflammatory
4 months EC
4-6 months Hp
6 months EC
18 months Hp

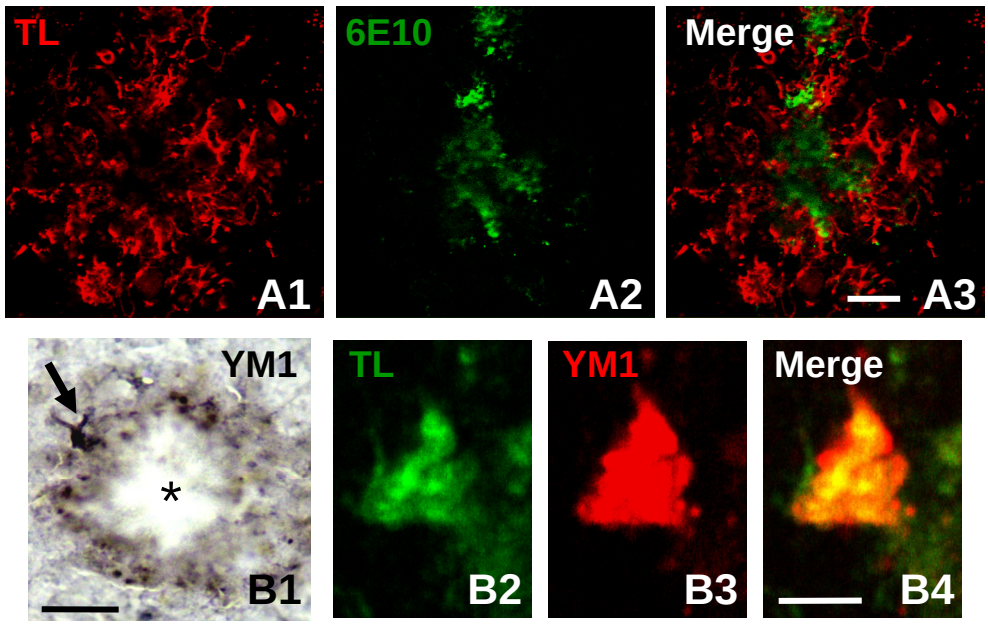

Supplemental Figure 1